UNIVERSITY OF CYPRUS

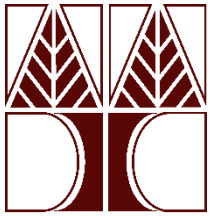

Master Thesis

Synthesis and Study of Thermal Stability of Thermoelectric Materials

Maria Theologou

DEPARTMENT OF MECHANICAL AND MANUFACTURING ENGINEERING

UNIVERSITY OF CYPRUS
DEPARTMENT OF MECHANICAL AND MANUFACTURING ENGINEERING

Synthesis and Study of Thermal Stability of Thermoelectric Materials

Maria Theologou

Supervisor:
Dr. Theodora Kyratsi

Table of Contents

Table of Figures

Table of Tables

1. Abstract

In the last decades, an enormous interest appears at the scientific community on the magnesium silicide type materials that exhibit remarkable thermoelectric properties. Environmental-friendliness, low cost, excellent thermoelectric properties, abundance of the elements, high reliability, and non-toxicity are the main reasons that magnesium silicides are considered for future use on high temperature power generation applications.

Furthermore, consumption of energy has become one of the most important issues worldwide. In addition to improving alternative energy sources, saving energy is also critical in order to satisfy the rapidly increasing demand. Additionally, transportation is considered one of the largest consumptions of energy. Evidently, three quarters of the energy used for transportation is wasted as heat released to the environment. Thermoelectric generators can offer an alternative solution since they can convert wasted heat to electricity. Since these applications are mainly working in medium temperature range, stability issues are extremely important for the lifetime of such devices.

The main purpose of this thesis was to study the thermal stability of highly efficient $Mg_2Si_{0.57}Sn_{0.4}Bi_{0.03}$ thermoelectric material. $Mg_2Si_{0.57}Sn_{0.4}Bi_{0.03}$ was synthesized by mechanical alloying and consolidated by hot press sintering. Thermal stability of the synthesized materials was tested by applying three different coatings on the samples, exposed at the same temperature conditions in two different atmospheres (air and argon). The coatings used were Bison, Soudal and Boron Nitride spray. The results showed that argon annealed samples were less affected from the heat treatment, compared to air annealed samples. Bison and Soudal coatings could not protect the synthesized material from oxidation and Mg loss during heat treatment. On the other hand, argon annealed samples with BN as well as without coating were less affected from the specific procedure. Finally, applying boron nitride coating seems an effective way to minimize oxidation and Mg loss from heat treatment procedure.

2. ***Acknowledgements***

From the beginning, the specific study was considered a great challenge for me. A lot of time and thoughts were devoted to the completion of this thesis. I learned many interesting things and I hope that I helped the future engineers who will continue this study or use it for their own knowledge purposes.

In that respect I would like to thank my wonderful family, who believe in me, always support me emotionally and financially to all my choices. Also, I would like to thank my supervisor Dr. Theodora Kyratsi for her consultation, support, encouragement, and patience. Furthermore, I would like to gratefully acknowledge Gianna Ioannou, Elli Symeou and George Mesaritis for their untiring support and guidance.

University of Cyprus, May 2021

3. ***Introduction***

Worldwide researches lead to the conclusion that from the primary energy consumption, only 34 per cent is successfully used. The remaining 66 per cent of the energy, is lost unjust and mostly in a waste of heat form. [1]

High performance thermoelectric (TE) materials, because of their extremely thermoelectric (TE) properties, have enormous potential applications at high and intermediate temperature thermoelectric (TE) devices. Main ability of high performance thermoelectric materials, is to convert heat energy to electrical energy directly and reversibly. An environment-friendly technology, as the thermoelectric device consist a practical and direct solution for the exploitation of the waste heat as much as possible. High reliability, feasibility in a wide temperature range and no pollutants are the main characteristics of a thermoelectric device.

At the last decades, an enormous interest is increased, about the p-type and the n-type Magnesium Silicide at the scientific community, highly due to its remarkable thermoelectric properties. Because of its environmental-friendliness, low cost, excellent thermoelectric properties, abundance, high reliability and non-toxic abilities, Magnesium Silicide consist of an extremely promising contestant, for future use to high temperature power generation applications.

The main purpose of the specific study is to obtain thermal stability and the synthesis of $Mg_2Si_{0.57}$ $Sn_{0.4}Bi_{0.03}$ material. $Mg_2Si_{0.57}$ $Sn_{0.4}Bi_{0.03}$ samples which were used at the experiment, were synthesized by Mechanical Alloying (MA) and consolidated by Hot Pressing.

The thermal stability of the material was tested by applying three different coatings on the samples, exposed in the same temperature conditions. Each coating had different heat resistance and was applied in two identical samples. Half of the samples were placed in a capsule which was sealed in an Argo atmosphere, for the argon annealing. The other half of the samples was placed in a glass test tube which was filled with an atmospheric air for the air annealing. Samples were tested at 723 K (450 °C) for 500 hours (21 days).

4. Background Theory

Last decades, consumption of energy has become one of the most important issues worldwide. An environmentally and a humanly friendly solution is Thermoelectric effect. Directly relevant with Thermoelectric (TE) materials are three effects, Thomson effect, Peltier effect and Seebeck effect. At the specific study mainly were used Peltier and Seebeck effects. Additionally, an efficient thermoelectric device needs a TE material with high figure of merit and thermal stability. For the purpose of the specific study, $Mg_2Si_{0.57}$ $Sn_{0.4}Bi_{0.03}$ was chosen. Main targets of the study were to synthesize $Mg_2Si_{0.57}$ $Sn_{0.4}Bi_{0.03}$ and to study its thermal stability.

4.1 Thermoelectric Effects

4.1.1 Seebeck Effect

When there is a temperature difference between two electrical semiconductors or conductors, which are also consist of a different conductive material, an electric current flow is produce due to the voltage difference that is produce between two substances. This specific phenomenon is called 'Seebeck Effect'. Seebeck Effect was first discovered in 1821, from German physicist Thomas Jihann Seebeck (1770-1831). Thomas Jihann Seebeck was tested various bimetallic contacts and recorded the behavior by associating it with a factor that took its name, Seebeck factor. The Seebeck Coefficient can be calculated by the following formulae.

$$S = -\frac{\Delta V}{\Delta T}$$

Where, the letters 'ΔV' represent the value of voltage difference (V) which is generated between the two conductive metals and the letters 'ΔT' represent the value of the temperature difference (^{0}C) between the hot and cold sides of the material. [3]

Materials of different Seebeck coefficients (n-doped and p-doped semiconductors), can compose a thermoelectric circuit which can configured as a thermoelectric generator. Seebeck effect phenomenon is responsible for the creation of the thermoelectric generator (TEG), also called a Seebeck generator, which converts temperature differences (heat flux) directly into electrical energy. Most common applications for thermoelectric generator are solar radiation, Industrial processes and automotive exhaust.

4.1.2 Peltier Effect

The reverse procedure of Seebeck effect can be achieved by the use of Peltier Effect. Peltier effect was first discovered in 1834, by French physicist Jean Charles Athanase Peltier.

To create an electric current between two joined conductors, a voltage must be applied. The current flows through the two conductor's junctions and heat is transfers from one junction to the other one. In that way, the temperature of the two electrical junctions can be decreased or increased, by creating that way a temperature difference between the two junctions. Peltier coefficients represents the amount of heat is carried per unit charge and its value can be calculated with the use of the following formulae. [5]

$$Q = (\Pi_A - \Pi_B) * J$$

Where, the symbols Π_A and Π_B are represent the Peltier coefficient's values of conductors A and B respectively. Also, the letter J represents the value of the electric current between the two conductors A and B.

Peltier effect phenomenon is responsible for the creation of thermoelectric coolers (TEC), which is creating a temperature differences (heat flux) between two different types of material's junction. Computer chips, Peltier air conditioners and climate-controlled jacket are some of the most common applications for thermoelectric coolers.

4.2 Thermoelectric (TE) Materials

Thermoelectric (TE) materials are separated in categories, depended on their processing temperature. First category includes Bismuth Tellurium (Bi_2Te_3) materials and its alloys, which can be used from room temperatures (25 ^{0}C) to 150 ^{0}C (298-423 K). Second category includes Silicon-Germanium ($Si_{1-x}Ge_x$) materials, which can be used in temperature values equals with the value of 1000 ^{0}C (727 K). Lastly, the last category includes Lead Tellurium (PbTe) materials and its alloys, which can be used in temperature values equals with the value of 700 ^{0}C (427 K). [23]

The development of the thermoelectric materials is separated in three generations. First generation includes thermoelectric materials with ZT value equals approximately to the value range of zero to one (ZT ~1) and efficiency value range 4-5%. Second generation includes thermoelectric materials with ZT value equals approximately to the value range of 1.3 to 1.7 (ZT ~1.3-1.7) and efficiency value range 11-15%. Lastly, third generation includes thermoelectric materials with ZT value equals approximately to the value range of 1.8 to 2.4 (ZT ~1.8-2.4) and efficiency value range 15-20%. [2]

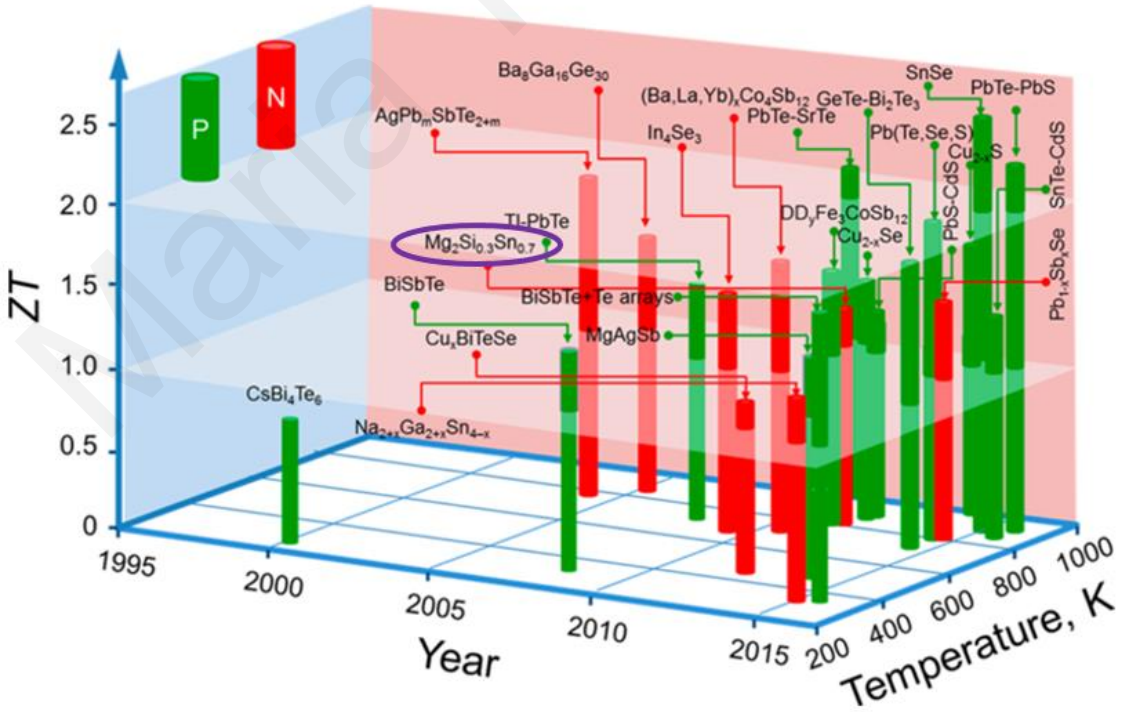

Figure 1Thermoelectric (TE) Material's ZT values [2]

As can be seen from figure 1, $Mg_2Si_{0.57}Sn_{0.4}Bi_{0.03}$ synthesis, which was used for the purpose of the specific thesis, is classified in the category of the second-generation thermoelectric materials, with ZT value equals approximately to the value range of 1.3 to 1.7 (ZT ~1.3-1.7) and efficiency value range 11-15%.

4.2.1 Figure of Merit ZT

Thermoelectric materials are including an enough wide range of solid compounds, because of their ability to convert temperature difference (thermal energy) to electricity (electrical energy). This specific ability of the thermoelectric materials creates two explicit technological applications. The first application is the generation of electrical energy from waste heat and the second one, the development of temperature gradients for cooling and heating devices.

The main essential properties of a fully valuable thermoelectric material are three. Low thermal conductivity value, high electrical conductivity value and high Seebeck coefficients. A low thermal conductivity will benefit to maintain a high temperature gradient and to retain heat at the junctions. Additionally, for the purpose of decrease Joule heating, the achievement of a high electrical conductivity value is essential. [4]

The conversion efficiency of a thermoelectric material can be measured with use of the dimensionless figure of merit, ZT. The figure of merit ZT can be calculated by the following formulae.

$$ZT = \frac{S^2}{\rho * \kappa} T$$

Where, the letter 'S' represents the value of Seebeck coefficient, the letter 'ρ' the value of electrical resistivity (Ω·m), the letter 'κ' the value of thermal conductivity (W/mK) and finally, the letter 'T' represents the value of the absolute temperature (°C). For the comparing of the possible efficiency values of different devices constructed different materials, ZT is considered a good convenient figure.

A considered good ZT value of a thermoelectric material must be equal to the value of 1 (ZT=1). Additionally, the best reported ZT values of different materials, are between the values of 2-3. If the value of ZT is equal with the range of 3-4, with regards to refrigeration and mechanical energy generation, would be an indispensability in order to be considered a good competitive in terms of efficiency value. However, no such ZT values have be achieved yet. [5]

4.2.2 Thermoelectric (TE) Element

By placing two thermoelectric (TE) material's pieces in parallel, a simple thermoelectric (TE) element can be made easily. One piece of the thermoelectric material must be n-type and the other one p-type. Both pieces must be placed in parallel, with their bottom and top surface connected electrically with an electric current through metal conductors. An n-type thermoelectric material has the ability to transfer heat in the opposite direction of the electric current. On the other hand, a p-type thermoelectric material, have the ability to transfer heat in the same direction where the electric current is supplied. [19]

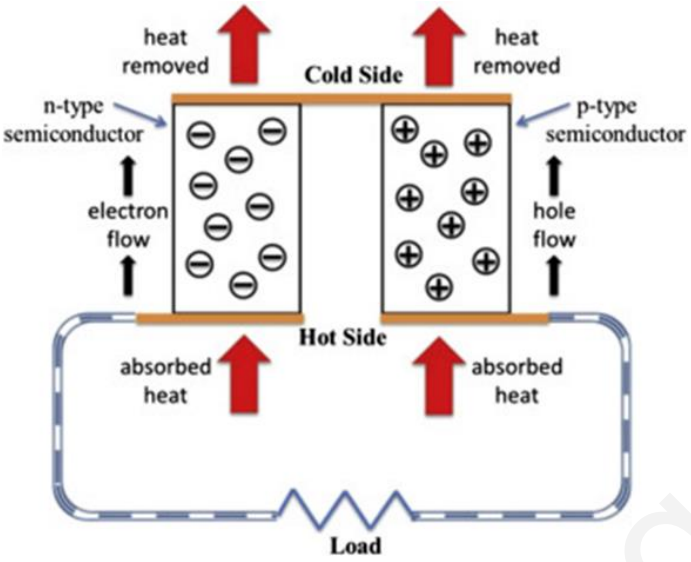

Figure 2Structure of a simple thermoelectric (TE) element [19]

As can be seen from the figure above, the structure of a simple thermoelectric (TE) element with n-type and p-type thermoelectric materials, can be arrange as shows. Additionally, is worth mentioning, that a thermoelectric element can be created with more than one combination of n-type and p-type thermoelectric materials. Can be created also, with only two n-type or with only two p-type pieces of thermoelectric materials. However, construction and electrical problems can be created very easily, due to the extremely complex wiring and the unwanted thermal bridges that formed from the metal pipes. In conclusion, the combination of one p-type and one n-type material, is the most workable and operating one. [20]

4.3 Thermoelectric (TE) Device and its Applications

4.3.1 Thermoelectric (TE) Device Structure

Thermoelectric (TE) module is consist by a number of n-type and p-type of thermoelectric (TE) elements, which are arrange in a row. The thermoelectric elements are connected electrically in series and thermally in parallel, as can see at the figure below.

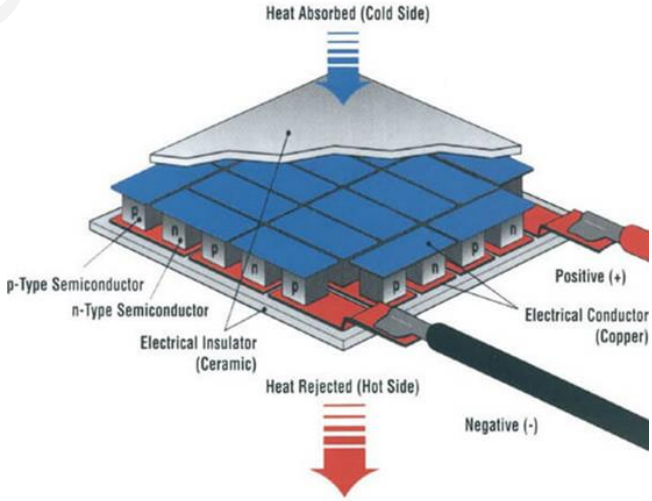

Figure 3Structure of Thermoelectric (TE) Element [20]

The electrical insulation of the thermoelectric elements and the transfer of the heat are succeeded by placing two ceramic plates. The specific ceramic plates are placed on the top and bottom surface of the thermoelectric module. [20] Also, there are thermoelectric (TE) devices, with a variety of heat pumping capacity, voltage, and operating temperatures. Very common, is the creation of thermoelectric modules with a multi number of pairs. With the addition of multi number of pairs at the thermoelectric device, it can be achieved an operation at lower voltage's values.

Figure 4Multistage Thermoelectric (TE) Device [21]

Thermoelectric (TE) devices have four main abilities which characterize them and make them a very good opponent for the solution of the wasted heat lost problem. Some of their many abilities, is the use of the wasted heat lost in order to generate electricity, have an extremely long life service, have no emissions (Environment friendly) and have no moving parts. Some of the most common thermoelectric device's applications are Electronic Devices Cooler, Thermoelectric Generators (TEG), Thermoelectric Refrigerator, Automobile System's Cooling and Air Conditioning. [22]

4.3.2 Applications of Thermoelectric Devices

Most common thermoelectric device's applications are Electronic Devices Cooler, Thermoelectric Generators (TEG), Thermoelectric (TE) Refrigerator, Automobile System's Cooling and Air Conditioning.

Thermoelectric Generator (TEG)

Seebeck Generator, also known as thermoelectric generator (TEG), has the ability to convert temperature difference (heat energy) into electrical power. The specific conversion can operate without the use of any rotating part/mechanism. According to Jangonda et al., thermoelectric generator applications for power plant of waste heat recovery and automobiles TEG, increase fuel efficiency. [40] Moreover, many applications of thermoelectric generator for automotives, aerospace, industrial, domestic, and thin film, have been reported from Zheng et al. [39]

Thermoelectric (TE) Refrigerator

Thermoelectric (TE) Refrigerator is using Peltier module to cool or to maintain at certain temperature, a particular space. According to some reported researchers, the COP of two stage or multistage thermoelectric (TE) modules is greater than the single stage TE refrigerator [40]. Over the past decades, the use of thermoelectric refrigerator or freezer for medical purpose such as

preservation/transportation of vaccination, blood serum and biological products have been reported. [39]

Electronic Devices Cooler

High power electronic devices such as computers, power amplifiers and microprocessors etc., because of their use in long intervals, large amounts of heat are produced within the system. That amount of heat can cause hardware failure and malfunction of the device. Consequently, with the use of an Electronic Device Cooler, the heat dissipates from the system and helps to enhance performance and lifespan of electronic devices. Traditional cooling systems cannot be used for cooling of electronic devices because they are not compact and have no space for their installation. Compact in size, no moving parts, less maintenance and use of DC supply to run, are some of thermoelectric cooler's advantages, in contrast with traditional cooling systems.

Automobile System's Cooling and Air Conditioning

In automobiles, there are many systems/devices such engines, exhaust systems, gear box, cooling systems etc, which produce heat. This waste of heat can be recovered with the use of Thermoelectric Generators (TEG). Over the past decades, many car manufacturing companies such as Renault, Honda, Ford etc, have developed their systems to use thermoelectric generators in order to recover exhaust heat losses. In addition, many automobile companies like Hyundai, Jaguar, Range Rover, Toyota, GM etc. are using thermoelectric modules to heat or cool car seats. [40]

It is worth mentioning, that because of Thermoelectric (TE) device's simplicity and portability, thermoelectricity applications have unlimited use and potential for further development.

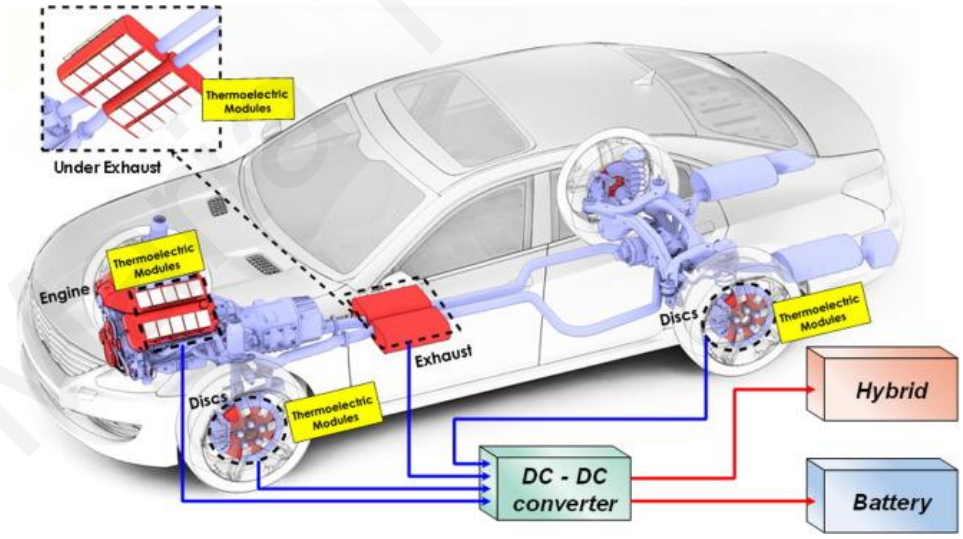

Figure 5Project's diagram of thermoelectric (TE) generator in a vehicle [41]

4.4 MgSi System

4.4.1 Mg_2Si- Compounds

In the last decades, consumption of energy has become one of the most important issues worldwide. In addition to improving alternative energy sources, saving energy is also critical in order to satisfy the rapidly increasing demand for energy. Furthermore, transportation is considered one of the largest uses of energy. More precisely, three quarters of the energy used for transportation is wasted as heat released to the environment. A solution is thermoelectric devices which can convert wasted heat to electricity. Mg_2Si has been recognized as a promising material for thermoelectric energy conversion at temperatures ranging from 500 to 800 K and has an enormous potential application in thermoelectric generators. [55] More specifically, because of its stability in the temperature range of functioning automobile exhaust (400–800 K), Mg_2Si considers a potential material for these applications.

Tellurium based thermoelectric materials, which are the most understood and developed materials operating in mid-temperature range of 500-800 K, are considered toxic and there is not enough supply of tellurium in the earth's crust to meet the needs for TEPG. On the other hand, silicon (Si), magnesium (Mg) and manganese (Mn) can all be obtained from the earth in large quantities. Furthermore, because of its low density, abundant and non-toxicity, Mg_2Si has an increased interest in scientific community as environmentally and humanly friendly material. [29]

Magnesium silicide (Mg_2Si) is an inorganic compound consisting of magnesium (Mg) and silicon (Si). The crystal structure of Mg_2Si is cubic, also called the antifluorite structure (Figure 6). As-grown Mg_2Si usually forms black crystals which they are semiconductors with n-type conductivity. [25]

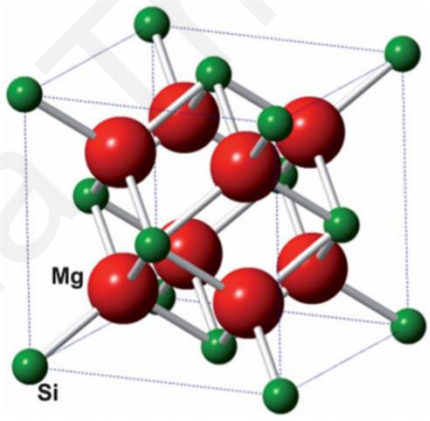

Figure 6 Cubic Structure of Mg_2Si (Green Color Spheres Indicate Si atoms and Red Indicate Mg) [32]

The specific material is suitable for structural applications due to its lightweight and thermophysical properties. [28] Mg_2Si is commonly used in the aerospace and the automobile industries. However, it seems that its use in automobile applications is much more promising, due its stability in the temperature range of functioning automobile exhaust (400–800 K). [26] Also, it is worth mentioning that as a material it is mainly characterized by its high specific elastic modulus and high specific strength. [27]

	Properties of Mg_2Si	
1	Molar Mass	76.695 g·mol^{-1}
2	Density	1.99 g cm^{-3}
3	Melting Point	1375 K (1102 °C)

Table 1Properties of Ng2Si

The specific material has a very important role in high temperature applications. It has been reported that Mg_2Si is an intermediate thermoelectric power generator material, since it is proved that its maximum operating temperature is equal to the value of 1000 K (727 ^{0}C). [30] Additionally, comparatively to compound telluride-based materials (e.g., PbTe) and skutterudite-based materials (e.g., $CoSb_3$), Mg_2Si has a fairly high thermal conductivity, which is above the value of 40 mW cm^{-1} K^{-1}. [31] Generally, the proposed silicide-based material alloys (e.g., Mg-Si, Mn-Si) can be used in the high temperature ranges where the Te based materials will fail by decomposition, sublimation, or even melting. Furthermore, Mg_2Si's Thermal Conductivity value, considers much higher value than typical good thermoelectric materials, such as $Yb_{14}MnSb_{11}$ (10 mW cm^{-1} K^{-1}) and $Bi_{2x}Sb_xTe_3$ (20 mW cm^{-1} K^{-1}). [36]

Additionally, Mg_2Si- compounds can be synthesized by two different methods, mechanical alloying, and solid-state reaction. However, it is very difficult to prepare the Mg_2Si by a melting process due to large difference in vapor pressures of the constituent elements and no solubility and because of a small difference between the boiling temperature of Mg (1380 K) and the melting temperature of Mg_2Si (1375 K). Therefore, it is difficult to control its composition, mainly due to volatilization and oxidation of Mg. [55]

The required working temperature for the specific material is approximately to the value of 773 K (500 ^{0}C). [32] Also, it is worth mentioning that the biggest ZT value of Mg_2Si compounds, has been reported at 900 K (627 ^{0}C), for $Mg_2Si_{0.55-x}Sn_{0.4}Ge_{0.05}Bi_x$ (ZT= 1, 4). [33]

4.4.2 $Mg_2Si_{0.6-x}Sn_{0.4}Bi_x$ compounds

Based on research, finest compositions of Solid solutions were found to be n-type $Mg_2Si_{0.6-x}Sn_{0.4}Bi_x$ compounds. [34] Of all the $Mg_2Si_{0.6-x}Sn_{0.4}Bi_x$ compounds, $Mg_2Si_{0.57}Sn_{0.4}Bi_{0.03}$ was chosen for the purpose of the specific study because of its admirable characteristics and TE properties. As all the Mg_2Si-Compounds, $Mg_2Si_{0.57}Sn_{0.4}Bi_{0.03}$ is non-toxic, which makes its use environmentally and humanly friendly. An important characteristic, such as the protection of the environment from the pollution and destruction is considered necessary.

Optimized composition of solid solution	Peak zT @ °C	Source
$Mg_2Si_{0.55-x}Sn_{0.4}Ge_{0.05}Bi_x$ for $x = 0.02$	1.4 @ 527 °C	Khan [43]
$Mg_2Si_{0.57}Sn_{0.4}Bi_{0.03}$	1.2 @ 577 °C	Kyratsi, Khan, Symeou, Vlachos [34]
$Mg_2Si_{0.55-x}Sn_{0.4}Ge_{0.05}Sb_x$ for $x = 0.0125$	1.2 @ 527 °C	Khan [43]
$Mg_2Si_{0.4}Sn_{0.6}$	1.1 @ 527 °C	Zaitsev [44]
$Mg_2Si_{0.6-x}Ge_{0.4}Bi_x$ for $x = 0.02$	1.0 @ 527 °C	Mars [45]
$Mg_2Si_{1-x}Bi_x$ for $x = 0.001$	0.81 @ 600 °C	Fiameni [46]
$Mg_2Si_{1-x}Bi_x$ for $x = 0.0015$	0.7 @ 502 °C	Bux [47]
$Mg_2Si_{0.59-x}Sn_{0.41}Sb_x$ for $x = 0.005$	0.68 @ 420 °C	Du [48]
$Mg_2Si_{1-x}Bi_x$ for $x = 0.03$	0.68 @ 537 °C	Ioannou [49]
$Mg_2Si_{1-x}Al_x$ for $x = 0.02$ + 0.25 vol.% glass-frit	0.6 @ 697 °C	Satyala [50]
$Mg_2Si_{1-x}Sb_x$ for $x = 0.02$	0.56 @ 589 °C	Tani [51]
$Mg_2Si_{1-x}Al_x$ for $x = 0.01$	0.50 @ 600 °C	Battiston [52]
$Mg_2Si_{0.6-x}Ge_{0.4}Ga_x$ for $x = 0.008$	0.36 @ 352 °C	Ihou-Mouko [53]

Figure 7Some optimized compositions of Magnesium Silicide, Mg_2Si-based Solid Solutions, and their corresponding Figure of Merit Values

Furthermore, the required materials to produce the specific compound are available in abundance, which makes it possible to be fabricated in large quantities and its production can be defined as a low-cost procedure.

Higher figure of merit which was ever reported for $Mg_2Si_{0.57}Sn_{0.4}Bi_{0.03}$ compound, is equal with the value of 1.2 (ZT=1.2) at a temperature of 850 K. Finest values of power factor and of thermal conductivity were reported at the values of 36 $\mu Wcm^{-1}*K^{-2}$ and at 1.5 $Wm^{-1}K^{-1}$, respectively. [34] Figure 7, represents some of the many different compositions and the achieved figure of merit data.

Additionally, two different synthetic approaches were explored for the fabrication of $Mg_2Si_{0.57}Sn_{0.4}Bi_{0.03}$ compound, ball milling (BM) followed by hot pressing and gas phase synthesis followed by SPS. Furthermore, a rapid chemical synthesis of nanocrystalline silicon was reported. [54]

One of the main objectives of the specific thesis is to obtain thermal stability of $Mg_2Si_{0.57}Sn_{0.4}Bi_{0.03}$ material. Except of a high figure of merit value, thermal stability of a thermoelectric material is necessary for a fully functional and efficient thermoelectric device. Polymer thermal stability can be obtained if the polymeric material has the ability to resist the action of heat and to maintain its properties, such as strength and toughness, at given temperature. [42]

Thermal stability of polymer depends mainly on its chemical structure, degree of crystallinity and molecular weight. Additionally, it is worth mentioning, that thermal stability of polymer is not just a function of temperature but also depends on the duration the material experiences these temperatures.

Many previous studies focus on the study of thermal stability of $Mg_2Si_{1-x}Sn_x$ compounds. Yin K., Zhang Q., Zheng Y. et al., explored the influence of annealing time, annealing temperature, annealing atmosphere, and preventing coating was made. Samples were tested for long periods of time and at temperature of 823 K. The study concluded that the use of BN sprays, can prevent steam corrosion and minimize oxidation of the samples at temperatures of about 800 K. [56] Farahi N., Stiewe C., Truong N. et al., have successfully synthesized large scale high efficiency $Mg_2Si_{0.3}Sn_{o.675}Bi_{0.025}$ samples by utilizing the combination of melting and ball milling techniques. Furthermore, the TE material samples were tested and verified for their stability at least 720 hours at 723 K. [57]

In the specific study, to understand the effect of heat treatment on the synthesized material, characterization of annealed samples structure, chemical compositions and thermoelectric properties were made. Also, three different types of preventing coatings were used, such as BN spray, Bison paste and Soudal paste.

5 Experimental Equipment and Procedure

$Mg_2Si_{0.57}Sn_{0.4}Bi_{0.03}$ was synthesized by Mechanical Alloying (MA) and consolidated by Hot Pressing (HP). For Thermal Stability test a number of specialized machines was used. For annealed samples structure characterization, X-ray Diffraction (XRD) and Scanning Electron Microscope (SEM) were used. Furthermore, for annealed samples Thermoelectric (TE) characterization, LFA 467 MicroFlash and Ulvac (ZEM-3) were used.

5.1 Experimental Equipment

5.1.1 Synthesis

Planetary Mono Mill Pulverisette 6

A Ball Mill is a type of grinder which is used to grind or blend materials and consists by a hollow cylindrical grinding bowl (vial) which rotates around its own axis on a main disk whilst rotating rapidly in the opposite direction. The vial's axis is usually placed horizontally or at a small angle horizontally. Inside of the Vial a number of grinding balls is placed. The comminuting of the material to be ground takes place primarily through the high-energy impact of grinding balls, which usually are made of steel (chrome steel), stainless steel, ceramic, or rubber.

Material is placed inside the grinding bowl (Vial) with the grinding balls. Vial starts to rotate around its own axis at a certain speed and centrifugal force is created. The centrifugal force causes the ground material and grinding balls to separate from the inner wall of the grinding bowl. By the impact to the opposite grinding bowl wall at high speed, grinding balls grind the placed material. Additionally, impact between the balls themselves on the material adds to the size reduction process.

Figure 8Planetary Mono Mill Pulverisette 6 [38]

For the Mechanical Alloying (MA) procedure of the specific study, a Planetary Mono Mill Pulverisette 6 was used. Planetary Ball Mill consists by a single hardened-steel vial which includes 25 stainless steel grinding balls (diameter 5 mm).

5.1.2 Thermal Stability Test

5.1.2.1 Structure Characterization

X-ray Diffraction (XRD)

In 1912, Max von Laue discovered that crystalline substances act as three-dimensional diffraction gratings for X-ray wavelengths similar to the spacing of planes in a crystal lattice. X-ray diffraction (XRD) is a very usual technique in material science which, can obtain information relating to the structure of crystalline materials by using on the X-ray's dual wave/particle nature.

For this procedure can be used many forms of samples, but the most commonly used for phase characterization of the synthesis, is the powder method. Powder method can easily obtain the differentiation between phases having different crystal structures but, same chemical composition. This specific technique is mostly used for identification of crystalline phases of unknown samples, for analysis, thin film characterization, for identification and characterization of synthesis based on their diffraction pattern. With the irradiating of X-rays to a material, XRD procedure can measure the scattering and intensities of X-ray's angles that the material leaves itself. [15]

These X-rays are generated by a cathode ray tube, filtered to produce monochromatic radiation, collimated to concentrate, and directed toward the sample. These diffracted X-rays are then detected, processed and counted. Due to the random orientation of the powdered material, all possible diffraction directions of the lattice should be attained by scanning the sample through a range of 2θangles. The interaction of the sample with incident rays, produces a diffracted ray when conditions satisfy Bragg's Law. Bragg's equation is as follows.

$$\eta\lambda = 2d * sin\theta$$

According to the derivation of Bragg's Law, the letter 'd' represents the distance between the atomic layers, the Greek letter 'λ' represents the wavelength of the incident X-ray beam and the letter 'n' as an integer. The specific formulae can give explanation of why the faces of crystals reflect X-ray beams at particular angles of incidence (Θ, λ). [15]

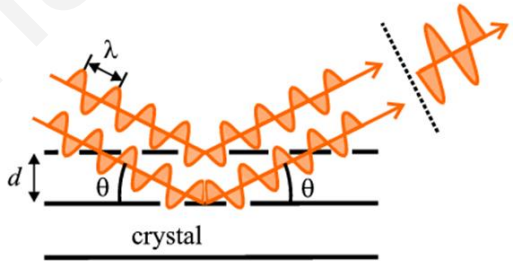

Figure 9 Explanation of Bragg's Law [35]

The wavelength of electromagnetic radiation to the diffraction angle and the lattice spacing are related by Bragg's Law, in a crystalline sample. Additionally, it is worth mentioning that X-rays can be considered as waves of electromagnetic radiation. Each Material consist by Crystals which can be considered as regular arrays of atoms. Because of the interaction with the atom's electrons, atom's Crystals scatter incident X-rays. This specific phenomenon is known as elastic scattering. A regular array of spherical waves can be produced by a regular array of electrons, also known as scatters. Through some

destructive interference that exist between the waves, the waves can cancel each other out, in many directions. However, in some specific directions, these waves can add constructively. Additionally, it is worth mentioning that each material can be recognized by its own unique array of waves, as humans have their own unique fingerprint. [16]

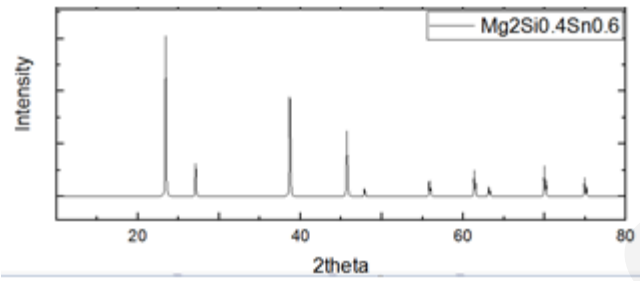

Figure 10X-ray Diffraction Pattern of Mg2Si0.4Sn0.6

Scanning Electron Microscope (SEM) / EDS

For a further analysis of the samples, a type of electron microscope was used, a Scanning Electron Microscope (SEM) which can be produced many of signal's types. For example, reflected or back-scattered electrons (BSE), characteristic X-rays, secondary electrons (SE), transmitted electrons and absorbed current (specimen current). By scanning sample's surface with a focused beam of electrons, scanning electron microscope (SEM) can produce images of the sample, which can obtain a more analytical view of the sample's microstructure, surface, and chemical elemental composition. [17]

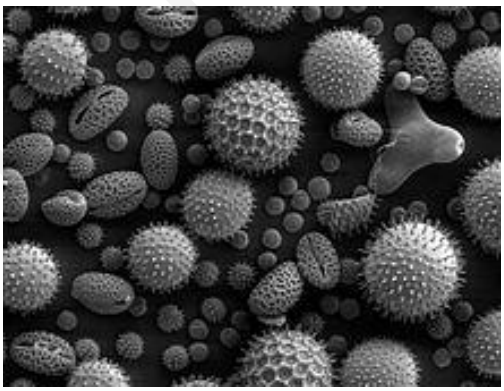

Figure 11 Image of pollen grains taken on SEM [18]

Signals are produced by the interaction between the electrons and the atoms in the sample. These specific signals obtain important information about the sample's composition and surface topography. The beam of electrons is scanned the sample's surface in a raster scan pattern. Additionally, in order to produce an image, the detected signal's intensity is combined with the electrons beam's position.

The use of a secondary electron detector, also known as Everhart-Thornley detector, on SEM is very common and with the Scanning Electron Microscope (SEM) in a common mode, can be easily detected secondary electron emitted by atoms excited by the beam of electrons. Additionally, from the sample's topography, signal's intensity and secondary electron's number are depended, which can be detected during the procedure. It is worth mentioning that some scanning electron microscopes (SEM), can achieve resolution greater that the value of one nanometer. [18] SEM/EDS provide information about material analysis that is not possible to obtain with other analytical techniques. In this work, SEM can be used for the study of annealed samples chemical composition and microstructure. For the microstructure analysis of annealed samples, a comparison between a non annealed sample and an annealed one is necessary.

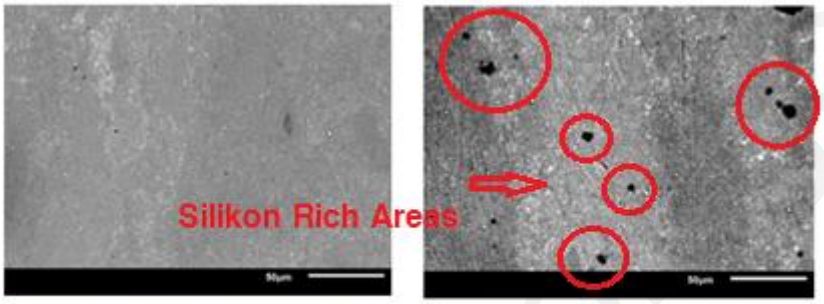

Figure 13Comparison between a non annealed Samples and an Annealed Samples Microstructure

Any difference between the annealed and the non annealed samples microstructure is information about heat treatment effect on samples. (Figure 13) Furthermore, the specific analytical technique can obtain information about the coating effect on the annealed samples surface. The main purpose of a coating use is to prevent oxidation and Mg loss of the samples, during heat treatment procedure. However, the use of a coating could negatively affect the annealed samples surface. A study of annealed samples surface's and coating's chemical composition, can obtain the effect of coating on the annealed sample. The specific analytical technique is known as cross-section. Figure 12 represents annealed sample's surface with coating, where light color area represents sample's surface and dark area represents coating's layer.

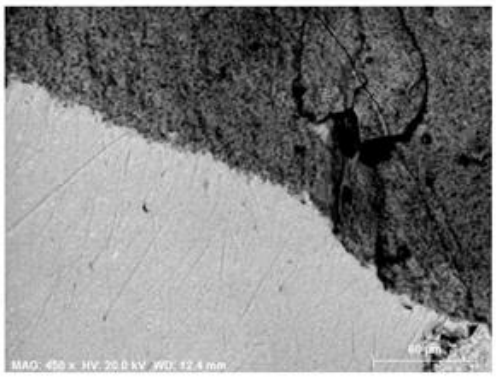

Figure 12Microstructure of Annealed Sample with Coating (Cross-Section)

5.1.2.2 Thermoelectric Characterization

LFA 467 MicroFlash

For the measurement of the specific heat (C_p) and the thermal diffusivity (a) of the samples, a LFA 457 MicroFlash was used. As can be seen from the figure below, LFA 457 MicroFlash is consists by seven main components, the Detector, the Iris, the Furnace, the Sample Carrier, the Furnace Hoist, the Electronics, and the Laser.

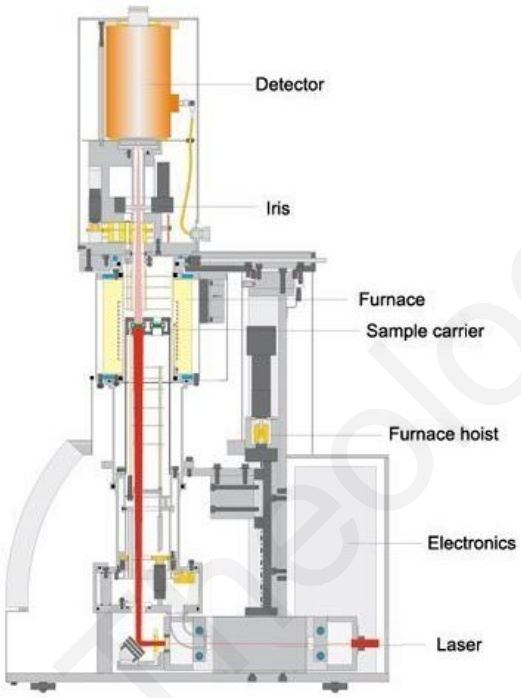

Figure 14 Schematic of LFA MicorFlash [9]

Laser Flash Analysis (LFA) also called, Light Flash Analysis, is used to analyze the thermal conductivity of a thermoelectric material, which is directly related to the thermoelectric material's efficiency. The laser flash method was firstly mentioned in studies in 1961 by Parker et al. Additionally, for the most effective use of any thermoelectric device, the knowledge of its thermal properties, it is essential. [9]

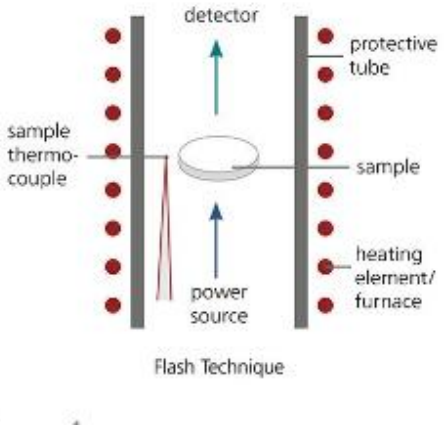

Figure 15Thermal Diffusivity (a) and Specific Heat (Cp) [9]

In order for the laser flash analysis (LFA) to take place, a plane parallel sample is placed inside of the device. As it can be seen on figure 15, while the measurement is carrying out, a short energy pulse or a short light is heating the sample's lower surface. As a result, there is a change at the temperature of the sample's upper surface. Then, with the use of an Infrared (RI) detector, the change of the temperature at the sample's upper surface, is measured multiple times.

Figure 16 represents the typical course of the signals. Signal is completely dependent by sample's thermal diffusivity. The higher the sample's thermal diffusivity, the steeper the signal increase.

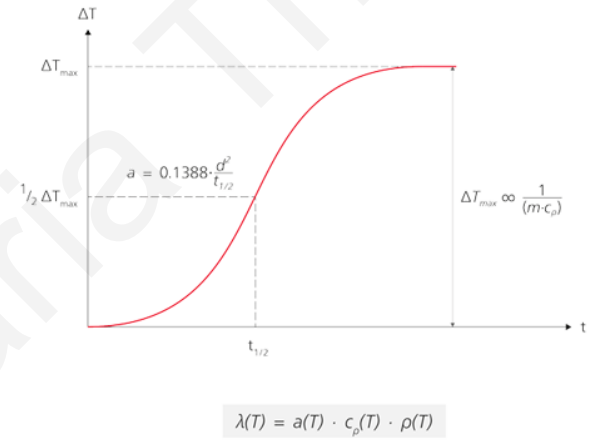

Figure 16Typical Course of Materials Signals [9]

The letter 'a' represents the value of Thermal Diffusivity, the letter 'ρ' the value of Density, the symbol 'Cp' the value of Specific heat capacity, the letter 'λ' the value of Thermal conductivity and finally, the letter 'T' represents the value of temperature. From the measured signals, the specific heat (C_p) and the thermal diffusivity (a) can be determined and with the value of density (ρ) known, the thermal conductivity (λ) can be calculated. [9]

Ulvac (ZEM-3)

For the electrical resistivity and the Seebeck coefficient measurement of the samples, a ZEM-3 unit (ULVAC) was used. This specific instrument operates by using the ‘’Small delta-t steady state’’ measurement method. The ZEM-3 instrument consists by a pc, a mobile rack with printer and a table top mounted base cabinet, which is also considered the main body of the instrument. As can be seen from the figure 17, the sample is placed inside the vacuum furnace, clamped between an upper and a lower block.

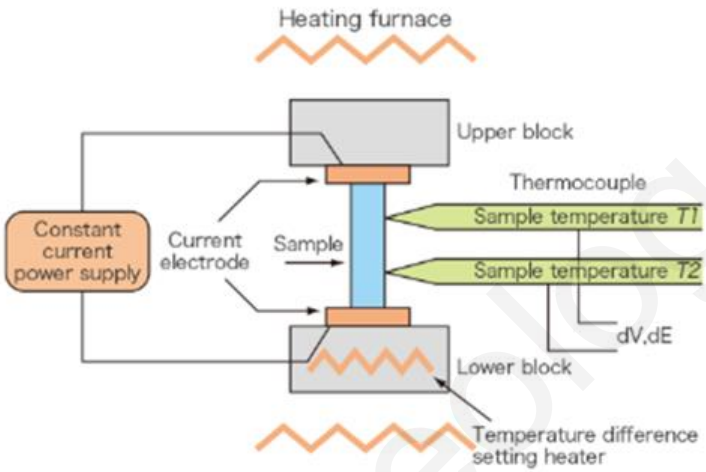

Figure 17 Structure of Ulvac's Vacuum Furnace [14]

For the electrical resistivity measurement, a constant power is applied and sends electrical current down through the sample. Then, one wire of each thermocouple probe is tapped in order to measure the voltage dropped when the electrical current flows through the sample.

For the Seebeck coefficient measurement, a small delta-t heater in the lower block, generates a thermal gradient across the sample. The temperature difference is measured by the two probes. As the electrical resistivity measurement’s procedure, one wire of each thermocouple measures the Seebeck voltage and temperature, which are being recorded by the thermocouple’s probes. [14]

5.2 Experimental Procedure
Electrical Resistivity

Electrical Resistivity, also called volume resistivity or specific electrical resistance, is a fundamental property of a material that defines how much strongly the chosen material will conducts or resists an electric current. [6] Specific units and formulas are used for electrical resistivity, in order for the resistivity values to be meaningful. Electrical Resistivity SI unit is the ohm meter (Ω·m) and its value usually representing by the Greek letter ‘ρ’. Electrical Resistivity value can be calculated with the use of the follow formulae.

$$\rho = \frac{E}{J}$$

Where, the Greek letter 'ρ' represents electrical resistivity of the material (Ω·m), the letter 'E' the magnitude of the electric field ($V \cdot m^{-1}$) and the letter 'J' the magnitude of the current density ($A \cdot m^{-2}$). The magnitude of the electric field across a material that gives a certain current density, is directly related for the definition of the resistivity value of the material. Furthermore, a material with low resistivity value, can easily allowed an electric current, unlike a material with high resistivity value. Materials that cannot conduct electric current easily are called insulators and the materials that can conduct electricity easily are called conductors. [7] Is worth mentioning that, Electrical Conductivity, also called specific conductance, represents the reciprocal of the electrical resistivity. Usually, is represents by the Greek letters 'σ', 'γ' and 'κ'. Additionally, electrical Conductivity SI unit is siemens per meter (S/m). [8]

Thermal Conductivity

Thermal Conductivity value represents and describes the ability of a material to conduct heat. Usually, is be denoted by the letters of 'κ', 'k' or 'λ' and can be measured with the unit of in Watt $m^{-1}K^{-1}$ (W/mK). Thermal Conductivity can be calculated with the use of the follow formulae.

$$\lambda = \alpha * C_p * d$$

Where the letter 'α' represents the value of thermal diffusivity (mm^2/s), the letter of 'Cp' the value of specific heat capacity (J/kgK) and the letter of 'd' represents the value of density which usually expressed in units of grams per cubic centimeter (g/cm^3). Specific heat capacity usually can express by the symbol ''Cp'' and its value express the capacity of a substance's sample divided by the sample's mass. Specific heat capacity of a substance can be expressed with the SI unit of Joules per kilogram and Kelvin (J/kgK) and can determine the amount of thermal energy which a material has the ability to store. Further, the value of Specific heat capacity (Cp) of a material can be measured with the use of Laser Flash Technique (LFA). [9] Thermal diffusivity (α) of a substance can be expressed with the SI unit of square millimeters to second (mm^2/s) and also, with the calculation of Thermal diffusivity (α) value, the rate of transfer of a material's heat can be measured from the hot end to the cold one.

Also, like the value of Specific heat capacity (Cp), the value of Thermal diffusivity (α) of a material can be determined also with the use of Laser Flash Technique (LFA) and can be measured by the following formulae.

$$\alpha = \frac{\mathrm{k}}{\rho * \mathrm{Cp}}$$

Where, the letter 'ρ' represents the value of density, the letter 'Cp' the value of specific heat. [10] Density value can express by the letter 'd' or the Greek letter 'ρ' and with the SI unit of kilograms per cubic meters (kg/m^3). Substance's Density (d) also, known as specific mass or volumetric mass density, express the value of its mass per volume and can be measured by the follow formulae.

$$\rho = \frac{m}{V}$$

In order for a material to be considered a good thermal conductor, is affected directly from its thermal conductivity value. As the thermal conductivity value of the material is high, the material can be

considered a better thermal conductor. [11] For the measurement of thermal conductivity there are many established measurements methods. Depending on thermal properties of each material, every measurement method is suitable for a specific range of materials. The most common method for the measurement of thermal conductivity of a material is the Laser Flash Analysis (LFA). [13]

5.2.1 Synthesize Procedure

$Mg_2Si_{0.57}Sn_{0.4}Bi_{0.03}$ was synthesized by Mechanical Alloying (MA) and consolidated by Hot Pressing (HP). For the preparation of $Mg_2Si_{0.57}Sn_{0.4}Bi_{0.03}$ samples, Silicon powder 99.999% (metals basis), Magnesium powder 99.8% (metals basis), Bismuth powder 99.999% (metals basis) and Tin powder 99.85% (metals basis) were used.

Table 2 Expected Experimental Values

$Mg_2Si_{0.57}Sn_{0.4}Bi_{0.03}$	
Expected Density Value	ρ = 2.6 - 2.7gr/cm^3
Expected Pellet Thickness	t= 2.2 mm

For the mechanical alloying (MA) procedure, a Planetary Mono Mill Pulverisette 6 and a hardened-steel vial which includes 25 stainless steel balls (diameter 5 mm) were used. The elements were placed together inside the vial, in an argon atmosphere due to element's flammable feature and in order to prevent the oxidation of the elements. The complete synthesis was achieved at 32 hours of ball milling (BM), at 400 rpm and at a weight ratio of 1:10. At the range of the 32 hours, every 8 hours of ball milling the procedure was stopped and inside an Argo atmosphere the synthesis was stirred in order to get the best result as possible. (Table 3)

Table 3Ball Milling (BM) Conditions

Ball Milling (BM) Conditions	
Time	32 hours
Speed	400 rpm
Milling Time	5 min of milling + 5 min pause
Reverse	On
Weigh Ratio	1:10

All samples were *hot-pressed* at 80 MPa (640 kg) for an hour, at a temperature of 863 K (590 ^{0}C). [34] Additionally, is worth mentioning that the density value of the samples, was measured to be equal with the value of 2,738 gr/cm^3 (ρ = 2,738 gr/cm^3) which is in the acceptable range ($\rho_{theoretical}$=2.6-2.7 gr/cm^3). (Table 2)

5.2.2 Heat Treatment Procedure

To have knowledge regarding the thermal stability of a material constitutes a very important element. With thermal stability of a material known, it will be more feasible the employ of the synthesized material's high efficiency for module fabrication. For this specific purpose, eight samples (with three different coatings) were extracted from the Ø 10 mm pellets and annealed. Half of the samples were

annealed in an atmospheric air and the other half, in an argon atmosphere. Additionally, in order to prevent oxidation and Mg loss of the samples as much as possible, three different types of coatings were used. [24] The coatings used were Bison (Paste 1), Soudal (Paste 2) and Boron Nitride (Spray). (Table 4) The inclusion of Boron Nitride (BN) coating was necessary, since it is considered a potent high temperature coating for $Mg_2Si_{0.57}Sn_{0.4}Bi_{0.03}$ samples, in order to prevent oxidation and Mg loss. [24]

	Coatings	***Characteristics***	***Properties***
1	Bison (Paste 1)	·Chemical base: Water glas ·Color: Black ·Consistency: Stable paste ·Density: 2 g/cm³ ·pH-value: approx. 12	·Heat resistant up to 1250 ^{0}C ·Forms a tough seam · Fire-proof sealing
2	Soudal (Paste 2)	·Chemical base: Sodium silicate ·Color: Light Grey ·Consistency: Stable paste ·Density 1,82 g/ cm³	·Heat resistant up to 1500 ^{0}C ·Free of asbestos ·Forms a tough seam · Fire-proof sealing
3	Boron Nitride (Spray)	·Chemical base: Ultra-High-Purity Boron Nitride ·Color: White ·Consistency: Spray	·Minimize Mg evaporation and prevent oxidation ·High temperature dry lubricant and release agent

Table 4 Experimental Coating's Characteristics

In order to obtain thermal stability of $Mg_2Si_{0.57}Sn_{0.4}Bi_{0.03}$ synthesized material, half of the samples were placed in a sealed capsule which was contain argon, for the annealing in argon atmosphere. The other half of the samples were placed in a sealed glass test tube for the air annealing. The glass test tube and the capsule were tested at 723 K (450 °C) for 500 hours (21 days). For each condition/coating of the heat treatment procedure, two identical samples were used.

6 Experimental Results and Discussion

For heat treatment procedure, half of the samples were argon annealed and the other half were air annealed. After heat treatment procedure, thermoelectric properties, chemical composition, and microstructure of annealed samples, were analyzed and characterized. Furthermore, a comparison was made between a non annealed sample and annealed samples, to study and to understand better heat treatment's effect on annealed samples.

6.1 Not annealed Sample (Ref.)

To study heat treatment's effect on annealed sample's thermoelectric properties, chemical composition and microstructure, a comparison with a non annealed sample is necessary. The specific sample must be made of the same synthesized material as annealed samples, but without go through the heat treatment procedure. For that purpose, an extra sample was made and was studied with the same technics as annealed samples were studied.

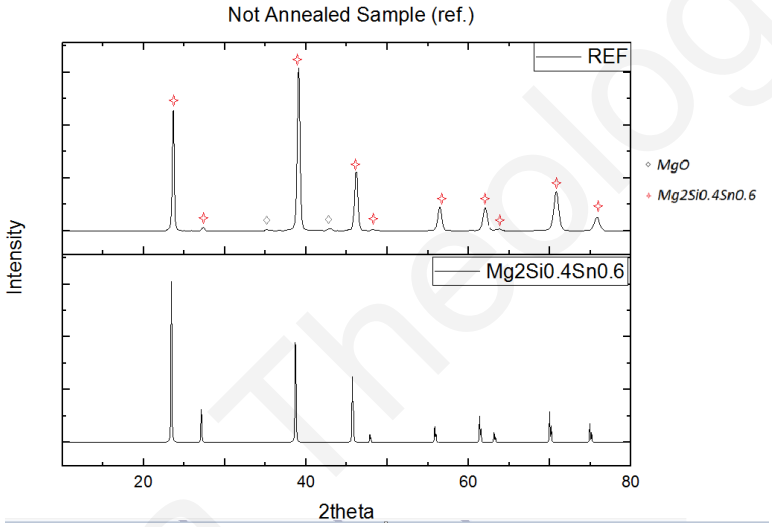

Figure 18Non Annealed Samples X-ray Diffraction Patterns

As can be seen from the non annealed sample's X-ray diffraction patterns, the sample has well-formed $Mg_2Si_{0.4}Sn_{0.6}$ solid solutions with high homogeneity. Furthermore, a small amount of MgO impurity can be observed, which is represented by a two weak diffraction peaks at $2\theta \approx 36^0$ and at $2\theta \approx 43^0$. (Figure 18) However, MgO impurity of the Mg_2Si-based materials is very common because of Mg's high volatility. Furthermore, Mg is highly reactive to residual oxygen at high temperature via oxidation process of every type of Mg_2Si-based compound. [34]

Table 5Non Annealed Samples Chemical Composition

NON ANNEALED SAMPLE (REF.)

				Nominal Composition
		Si	***Sn***	***Bi***
		0.57	0.40	0.03
				Chemical Composition
	Area	***Si***	***Sn***	***Bi***
Non Annealed (ref.)	Black	0.64	0.34	0.03

	Matrix	0.57	0.40	0.04

Table 5 represent the chemical composition of non annealed sample in comparison with the nominal composition. As it can be observed from the table above, there is no difference between nominal and chemical composition's stoichiometry. Generally, non annealed sample is homogeneous with very small Silicon rich areas (black areas) (Figure 19). This can be verified also from the non annealed sample chemical composition, which compared to nominal composition, there are a very small increase at Silicon (Si) values and consequently a very small decrease at Tin (Sn) values. (Table 5)

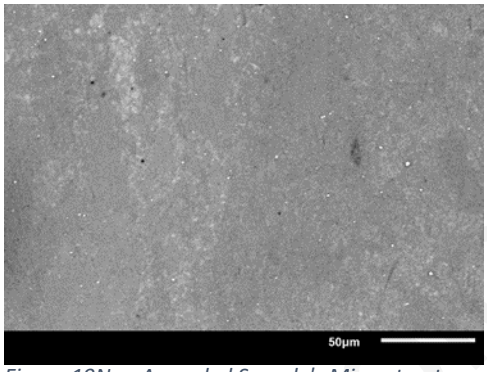

Figure 19Non Annealed Sample's Microstructure

Thermoelectric properties such as Electrical Conductivity (S/cm), Power Factor (µV/mK^2) and Seebeck Coefficient (µV/K) as a function of temperature (K) are shown below (Figures 20, 21 and 22). As it can be seen from the graphs, synthesized material TE properties are not as expected. A decrease at Thermal conductivity and Seebeck Coefficient values can be observed. Low Thermal Conductivity value shows material's poor ability to conduct an electric current. Low Seebeck Coefficient value shows synthesized material poor ability to create a voltage between the cold and the hot sample's ends. Additionally, Power Factor value is not at the desire level, as it is affected directly from Seebeck Coefficient and Thermal Conductivity values. Those values significantly affect negatively synthesize material TE performance. Furthermore, as was mentioned above, for an efficient TE material, Seebeck Coefficient value needs to be increased.

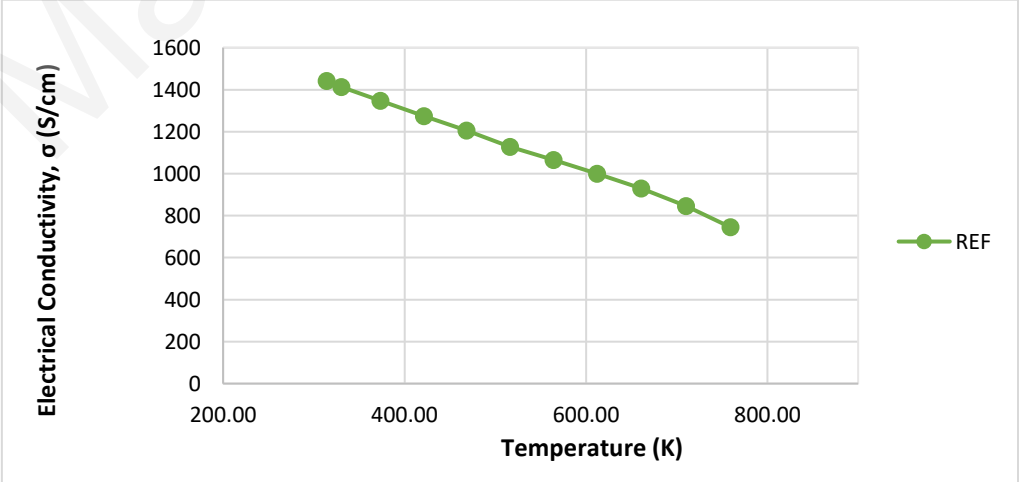

Figure 20Electrical Conductivity against Temperature (Non Annealed Sample)

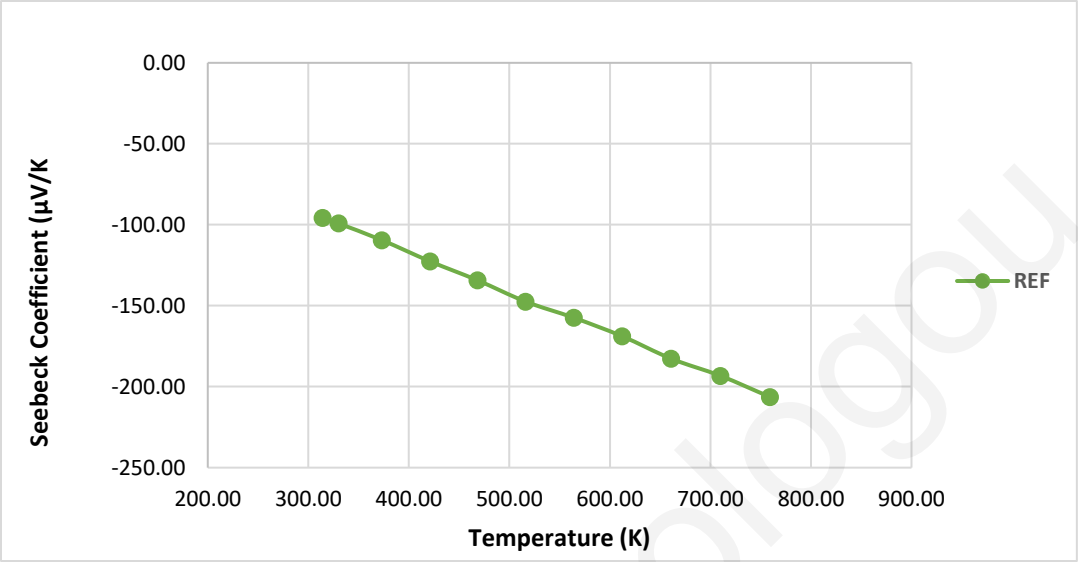

Figure 21Seebeck Coefficient against Temperature (Non Annealed Sample)

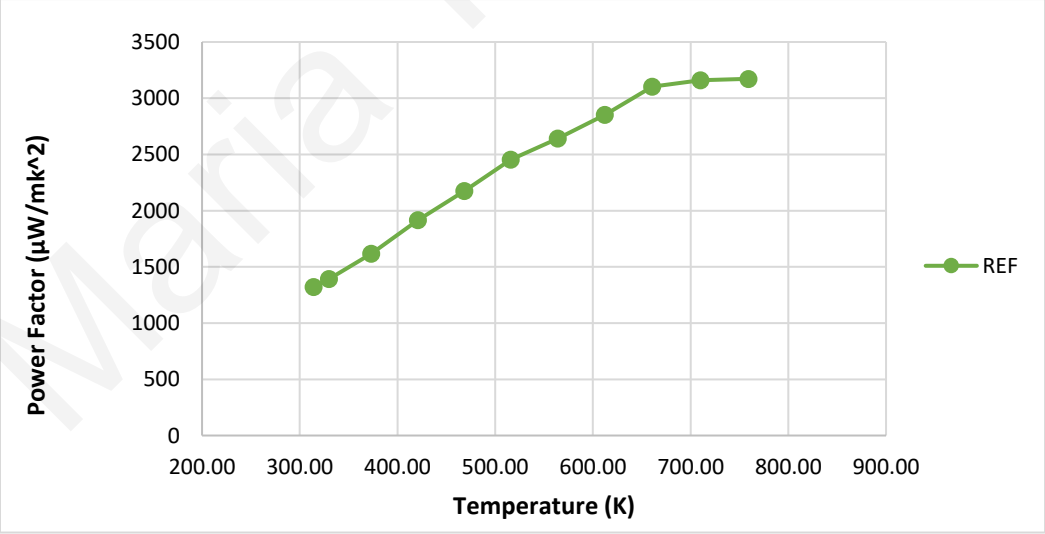

Figure 22Power Factor against Temperature (Non Annealed Sample)

6.2 Argon Annealed Samples

Thermal Stability of argon annealed samples was studied with specialized laboratory equipment. An X-ray Diffraction (XRD) was used to study argon annealed sample's structure. Argon annealed samples chemical composition and microstructure were studied with the use of a Scanning Electron Microscope (SEM). Additionally, to study thermoelectric properties of argon annealed samples, an Ulvac (ZEM-3) was used.

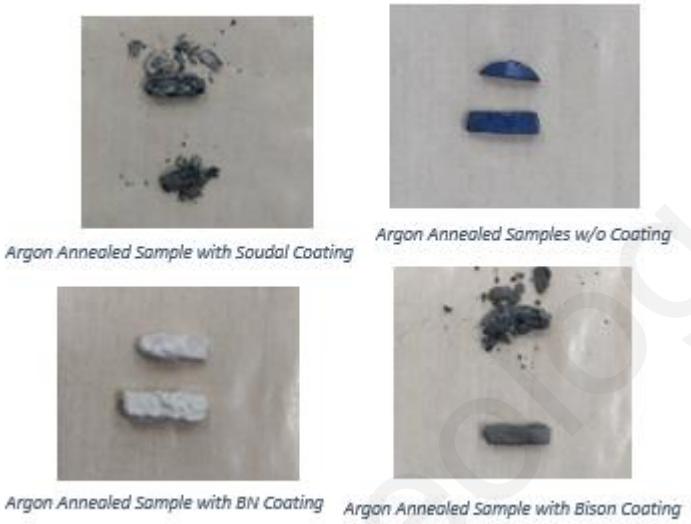

Figure 23Argon Annealed Samples after Heat Treatment

After heat treatment, argon annealed samples with BN coating and w/o coating maintained their original form, in contrast with argon annealed samples with Soudal and Bison coating which were deformed. Argon annealed samples with Soudal and Bison coatings, formed many cracks on the entire surface. Because of the cracks, the specific samples were very fragile and by applying small pressure, both samples bisected into smaller pieces. (Figure 23)

6.2.1 X-ray Diffraction (XRD) Patters of Argon Annealed Samples

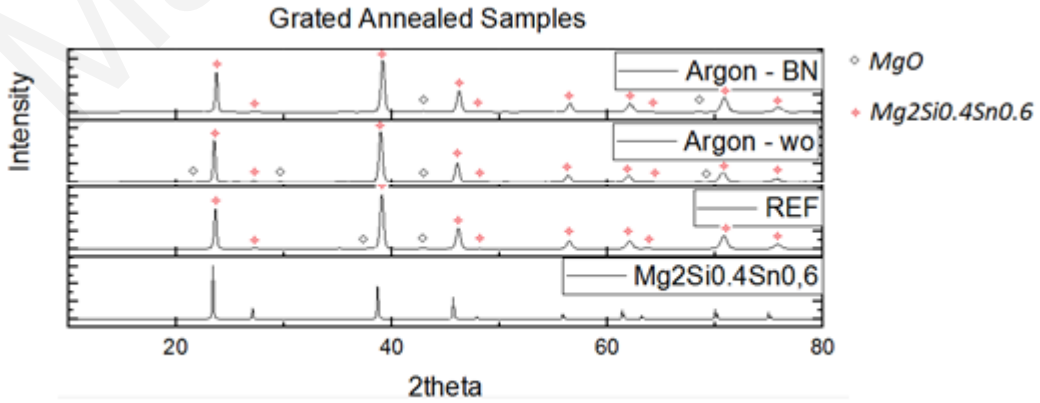

Figure 24Grated Argon Annealed Samples X-ray Diffraction Patterns

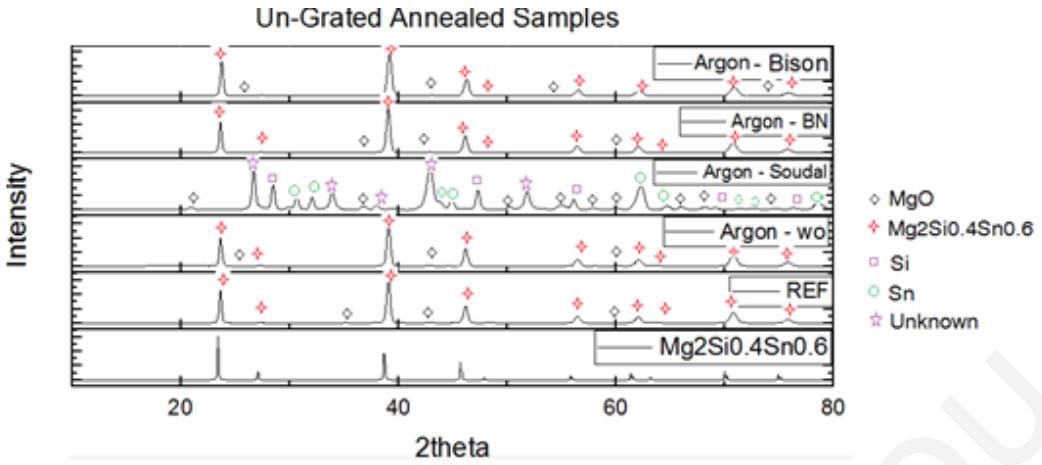

Figure 25Un-grated Argon Annealed Samples X-ray Diffraction Patterns

All grated argon annealed samples have well-formed $Mg_2Si_{0.4}Sn_{0.6}$ solid solutions with high homogeneity, which can be clearly observed across charts (Figures 24 and 25). Throughout the entire sample's heat treatment, a small amount of MgO impurity can be observed, which is represented by a weak diffraction peak at $2\theta\approx43^0$. It is important to note however, that for all the Mg_2Si-based materials, MgO impurity is very common, as mentioned. Un-grated argon annealed samples, with BN, Bison and w/o coating have well-formed $Mg_2Si_{0.4}Sn_{0.6}$ solid solutions with high homogeneity. However, compared with other argon annealed samples, argon sample with Soudal coating (un-grated), has formed different solid solutions (Figure 25). A bigger amount of MgO impurity and solid solutions of Si and Sn was formed in contrast to other annealed samples. Moreover, Sn and Si are represented mainly by a big diffraction peak at $2\theta\approx28^0$ and by smaller diffraction peak at $2\theta\approx62^0$, respectively. Additionally, a big amount of an unknown material is formed, which is represented mainly by two big diffraction peaks at $2\theta\approx27^{0,}$ and $2\theta\approx42^0$ (Figure 25). As mentioned above, the sample was deformed completely after the heat treatment. The formed of an unknown material in the specific argon annealed sample, confirms the fact that Soudal coating could not protect the sample from the heat treatment procedure.

6.2.2 Microstructure and Chemical Composition of Argon Annealed Samples (SEM)

Table 6Grated Argon Annealed Samples Chemical Composition

GRATED ANNEALED SAMPLES

					Nominal Composition
			Si	***Sn***	***Bi***
			0.57	0.40	0.03
					Chemical Composition
		Area	***Si***	***Sn***	***Bi***
	Non annealed (ref.)	Black	0.64	0.34	0.03
		Matrix	0.57	0.40	0.04
Argon Annealed Samples					
	Coatings	***Area***	***Si***	***Sn***	***Bi***

1	w/o	Black	0.58	0.39	0.03
		Matrix	0.57	0.39	0.03
2	BN	Black	0.62	0.36	0.03
		Matrix	0.60	0.37	0.03
3	Bison	Black	0.61	0.36	0.03
		Matrix	0.52	0.35	0.13

Table 7Un-grated Argon Annealed Samples Chemical Composition

UN-GRATED ANNEALED SAMPLES

					Nominal Composition
			Si	***Sn***	***Bi***
			0.57	0.40	0.03
					Chemical Composition
		Area	***Si***	***Sn***	***Bi***
	Non annealed (ref.)	Black	0.64	0.34	0.03
		Matrix	0.57	0.40	0.04
Argon Annealed Samples					
	Coatings	***Area***	***Si***	***Sn***	***Bi***
1	w/o	Black	0.59	0.40	0.02
		Matrix	0.58	0.40	0.02
2	BN	Black	0.62	0.36	0.02
		Matrix	0.59	0.39	0.03
3	Bison	Black	0.93	0.07	0.003
		Matrix	0.76	0.23	0.02

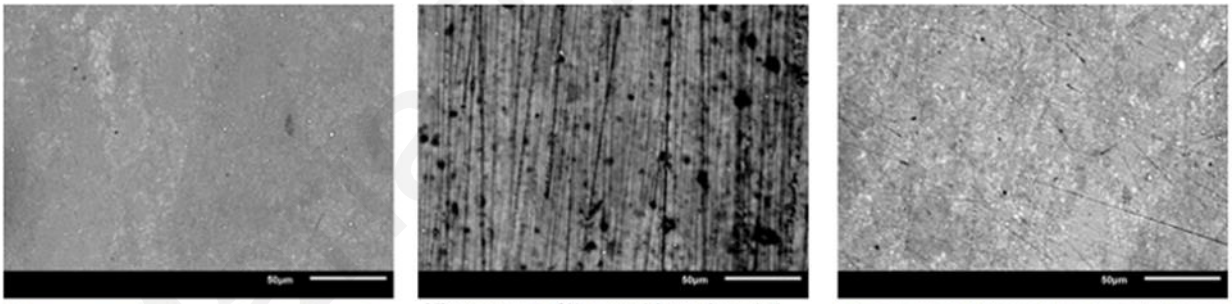

Microstructure of Reference's Sample (Grated) *Microstructure of Un-grated Argon Annealed Sample with BN Coating* *Microstructure of Grated Argon Annealed Sample with BN Coating*

Figure 26Microstrucutre of Argon Annealed Sample with BN Coating

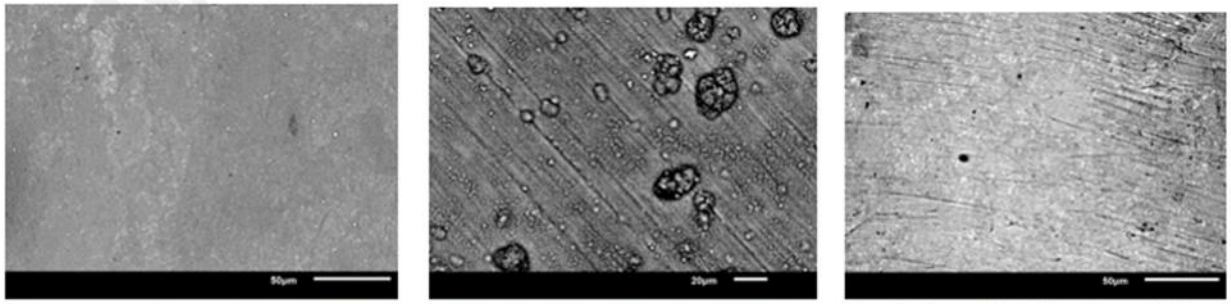

Microstructure of Reference's Sample (Grated) *Microstructure of Un-grated Argon Annealed Sample w/o Coating* *Microstructure of Grated Argon Annealed Sample w/o Coating*

Figure 27Microstructure of Argon Annealed Samples w/o Coating

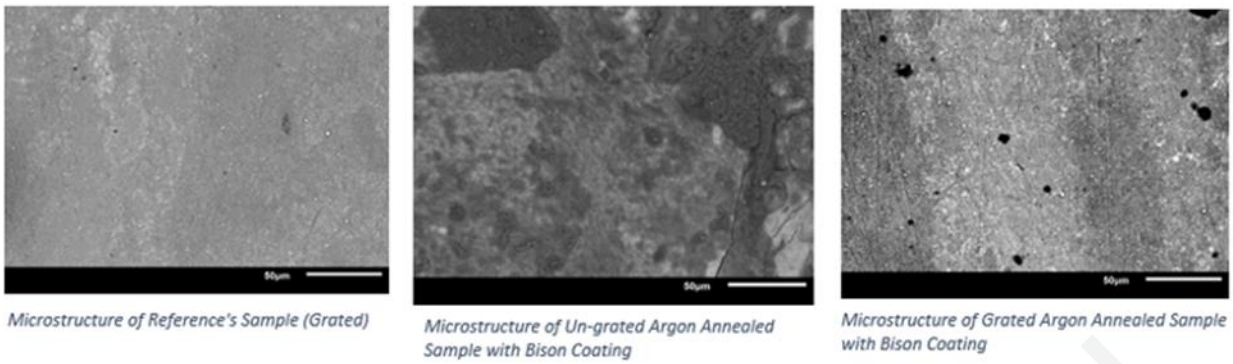

Figure 29Microstructure of Argon Annealed Sample with Bison Coating

Tables 6 and 7 above, represent the chemical composition of grated argon annealed samples and of un-grated argon annealed samples, respectively. Generally, argon annealed samples are homogeneous with Silicon rich areas (black areas), after the heat treatment procedure (Figures 26, 27 and 29). Additionally, as it can be seen from the chemical composition of the un-grated argon annealed samples, there is no change of material's stoichiometry after the heat treatment procedure (Table 7). Also, it can be observed, that grated annealed samples with Bison coating and w/o coating have form more Silicon rich areas (black areas) in contrast to grated annealed sample with BN coating. Furthermore, comparatively with the other argon annealed samples, sample with Bison coating have bigger Silicon rich areas (black areas). This can be verified also from the un-grated argon annealed samples chemical composition, where compared to nominal composition, there is an important increase at Silicon (Si) values and consequently an important decrease at Tin (Sn) values.

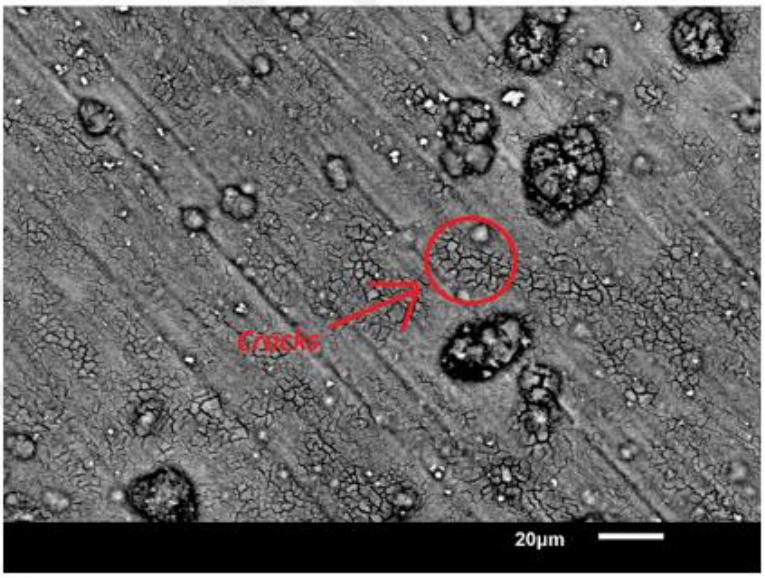

Figure 28Microstrucutre of Un-grated Argon Annealed Sample (w/o coating)

It is worth mentioning, that by studying the microstructure of the un-grated argon annealed samples, many small cracks are visible. It can be verified from this specific fact that some of the samples formed small cracks on their entire surface during the heat treatment, as reported above. (Figure 28) These specific results leading us to the conclusion, that Soudal and Bison coating, could not protect the argon annealed samples from oxidation after the heat treatment, so it is not possible to use them.

6.2.3 Thermoelectric (TE) Properties of Argon Annealed Samples

Measuring thermoelectric (TE) properties of the argon annealed samples after the heat treatment procedure is considered important step, to understand better the effect of heat treatment at the synthesized material. The key thermoelectric properties of argon annealed samples such as Electrical Conductivity (S/cm), Power Factor (μV/mK^2) and Seebeck Coefficient (μV/K) as a function of temperature (K) are shown. (Figures 30, 31 and 32)

Taking into consideration of Electrical Conductivity and Power Factor parameters, between argon annealed samples with BN and w/o coating, the sample with BN coating is the least affected. Electrical Conductivity and Seebeck Coefficient parameters have error range equal with the value of ±5%. On the other hand, Power Factor parameter has error range equal with the value of ±10%. As it can be observed from the graphs below both of argon annealed samples are in the acceptable range. (Figures 30, 31 and 32) However, in terms of Electrical Conductivity parameter, only argon annealed sample with BN coating is in the acceptable range (±5%). (Figure 31)

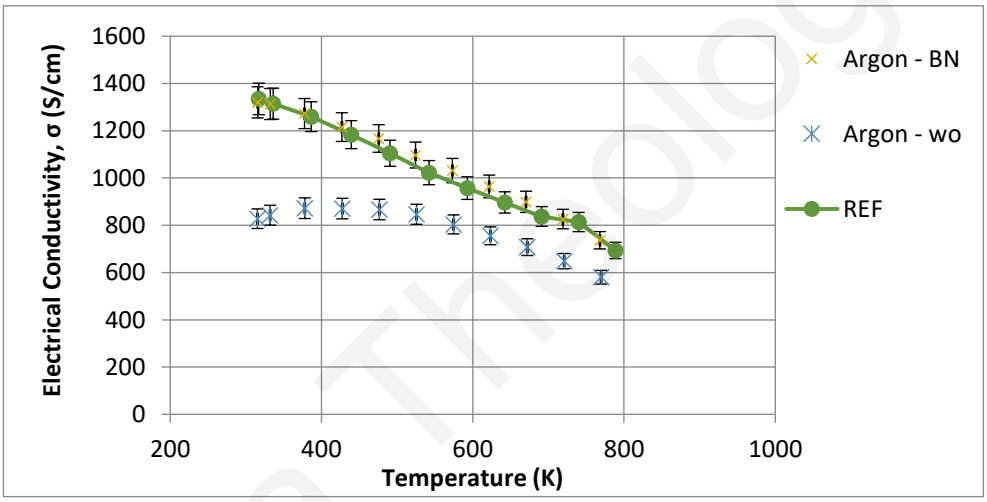

Figure 31Electrical Conductivity against Temperature (Argon Annealed Samples)

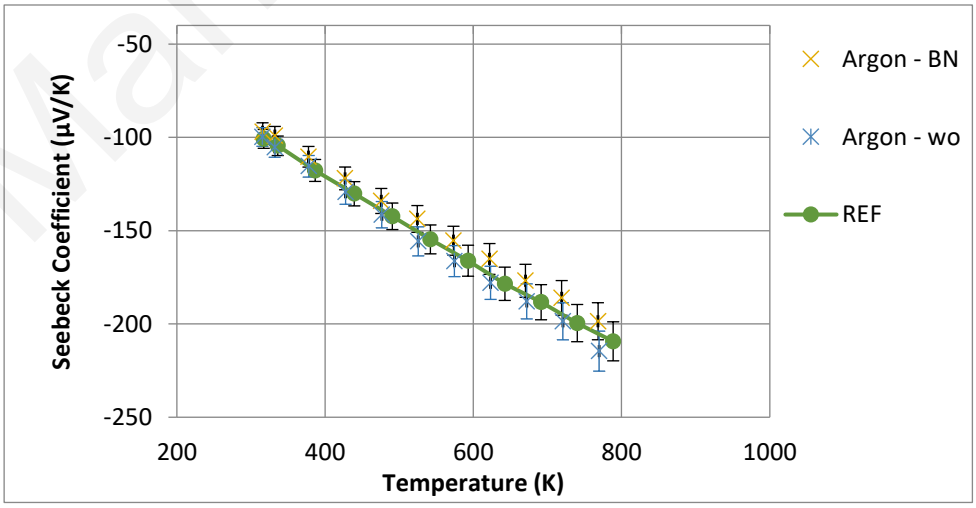

Figure 30Seebeck Coefficient against Temperature (Argon Annealed Samples)

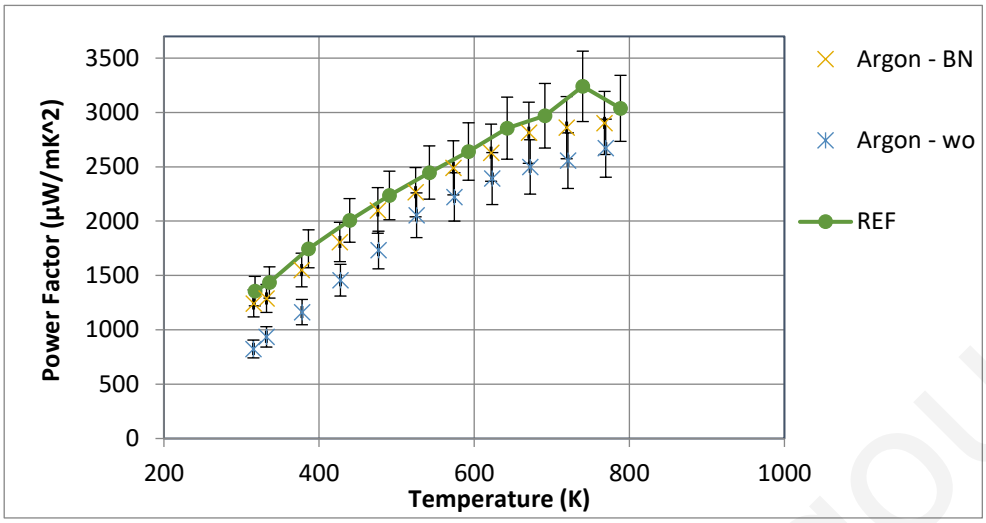

Figure 32Power Factor against Temperature (Argon Annealed Samples)

6.3 Air Annealed Samples

As argon annealed samples, thermal Stability of Air annealed samples was studied with same procedure. A specialized laboratory equipment was used. To study air annealed sample's structure, an X-ray Diffraction (XRD) was used. Also, a Scanning Electron Microscope (SEM) was used to study air annealed samples chemical composition and microstructure. Furthermore, an Ulvac (ZEM-3) was used to study thermoelectric properties of the air annealed samples.

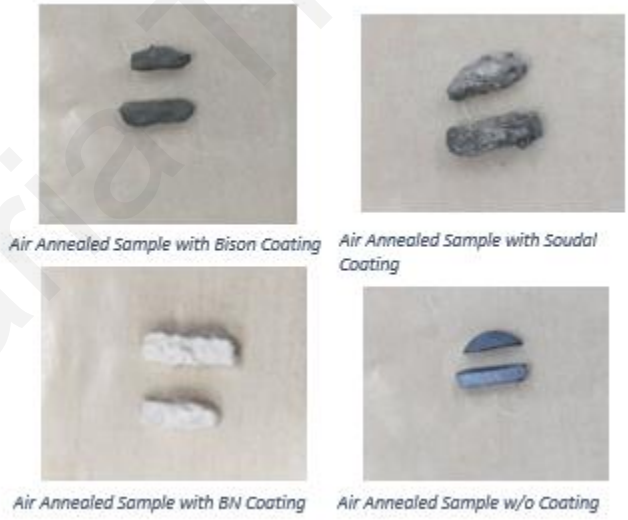

Figure 33Air Annealed Samples after Heat Treatment

After heat treatment, air annealed samples with BN coating and w/o coating maintained their original form, in contrast with air annealed samples with Soudal and Bison coatings which were deformed. Air annealed samples with Soudal and Bison coatings, formed many cracks on the entire surface. Because

of the cracks, the specific samples were very fragile and by applying small pressure, both samples bisected into smaller pieces. (Figure 33)

6.3.1 X-ray Diffraction (XRD) Patters of Air Annealed Samples

All air annealed samples have well-formed $Mg_2Si_{0.4}Sn_{0.6}$ solid solutions with high homogeneity, which can be clearly observed across all charts (Figures 34 and 35). After sample's heat treatment, a small amount of MgO impurity can be observed, which is represented by a weak diffraction peak at $2\theta \approx 43^0$. It is important to note however, that for all the Mg_2Si-based materials, MgO impurity is very common. All annealed samples contain a small amount of MgO. However, air annealed samples contain a bigger amount of MgO compared to argon annealed samples.

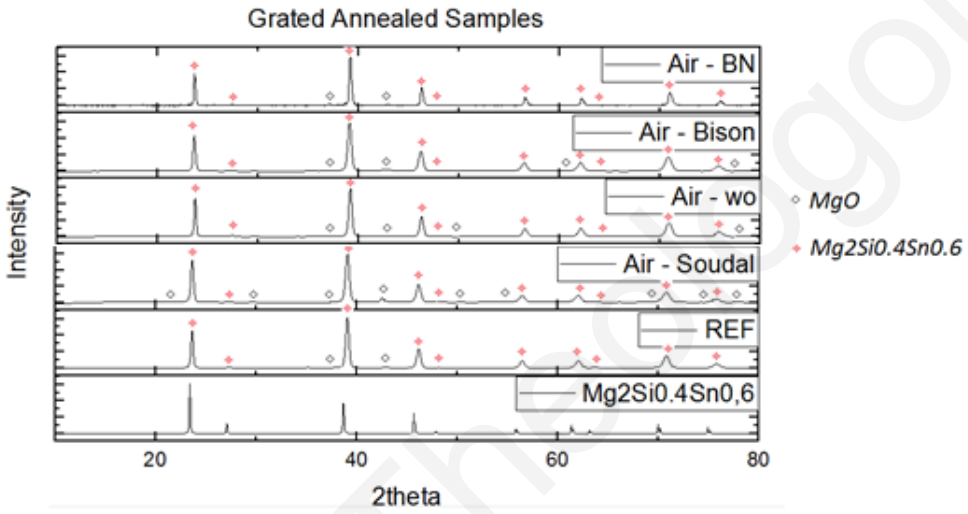

Figure 34Grated Air Annealed Samples X-ray Diffraction Patterns

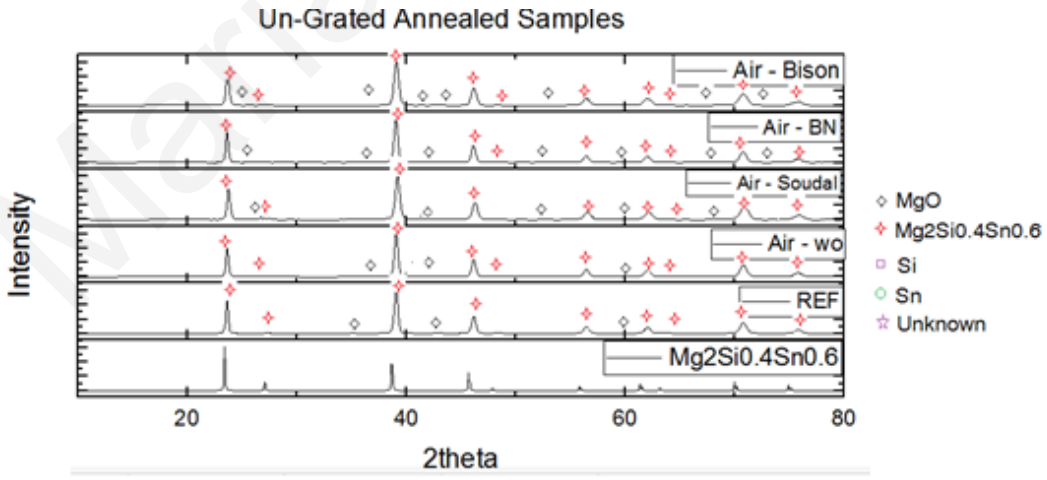

Figure 35Un-grated Air Annealed Samples X-ray Diffraction Patterns

6.3.2 Microstructure and Chemical Composition of Air Annealed Samples (SEM)

Table 8Grated Air Annealed Samples Chemical Composition

GRATED ANNEALED SAMPLES

					Nominal Composition
			Si	***Sn***	***Bi***
			0.57	0.40	0.03
					Chemical Composition
		Area	***Si***	***Sn***	***Bi***
	Non annealed (ref.)	Black	0.64	0.34	0.03
		Matrix	0.57	0.40	0.04
Air Annealed Samples					
	Coatings	***Area***	***Si***	***Sn***	***Bi***
1	w/o	Black	0.61	0.36	0.03
		Matrix	0.59	0.38	0.03
2	BN	Black	0.65	0.33	0.02
		Matrix	0.64	0.33	0.03
3	Bison	Black	0.57	0.40	0.03
		Matrix	0.55	0.41	0.04
4	Soudal	Black	0.57	0.40	0.04
		Matrix	0.55	0.41	0.04

Table 9Un-grated Air Annealed Samples Chemical Composition

UN-GRATED ANNEALED SAMPLES

					Nominal Composition
			Si	***Sn***	***Bi***
			0.57	0.40	0.03
					Chemical Composition
		Area	***Si***	***Sn***	***Bi***
	Non annealed (ref.)	Black	0.64	0.34	0.03
		Matrix	0.57	0.40	0.04
Air Annealed Samples					
	Coatings	***Area***	***Si***	***Sn***	***Bi***
1	w/o	Black	0.54	0.43	0.03
		Matrix	0.57	0.41	0.03
2	BN	Black	0.65	0.33	0.02
		Matrix	0.64	0.33	0.03
3	Bison	Black	0.95	0.04	0.002
		Matrix	0.80	0.19	0.01
4	Soudal	Black	0.99	0.01	0
		Matrix	0.66	0.32	0.03

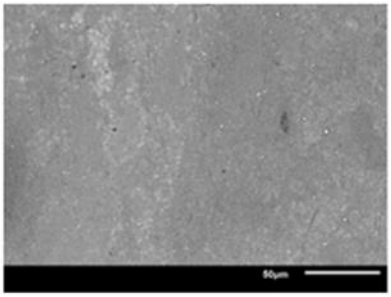

Microstructure of Reference's Sample (Grated)

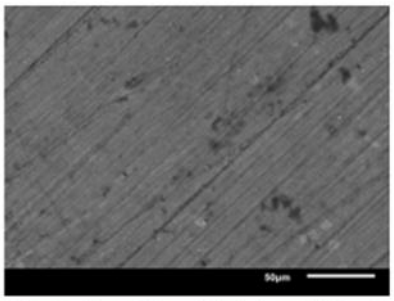

Microstructure of Un-grated Air Annealed Sample with Soudal Coating

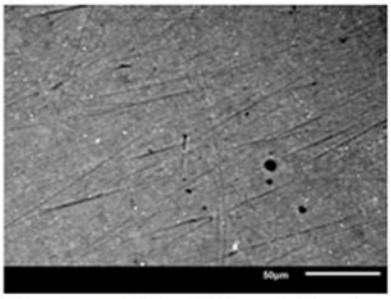

Microstructure of Grated Air Annealed Sample with Soudal Coating

Figure 39Microstructure of Air Annealed Sample with Soudal Coating

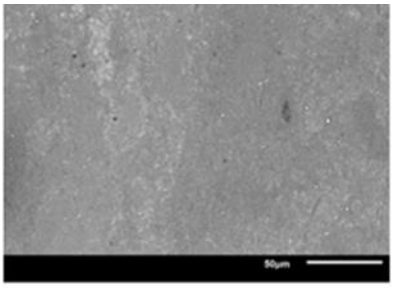

Microstructure of Reference's Sample (Grated)

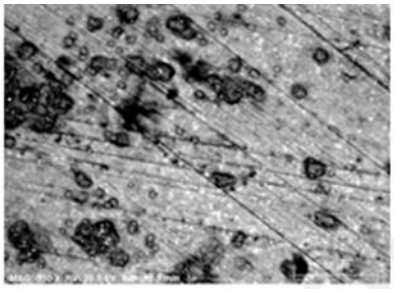

Microstructure of Un-grated Air Annealed Sample with BN Coating

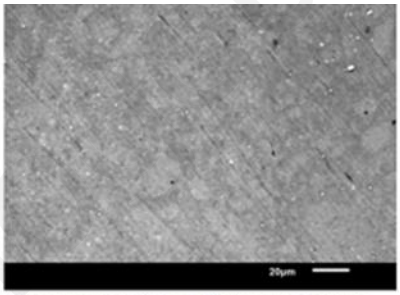

Microstructure of Grated Air Annealed Sample with BN Coating

Figure 38Microstructure of Air Annealed Sample with BN Coating

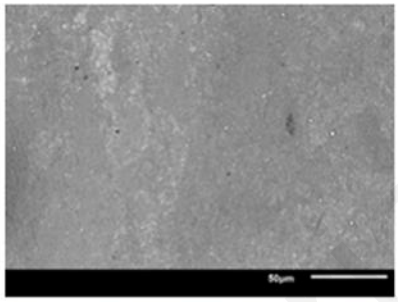

Microstructure of Reference's Sample (Grated)

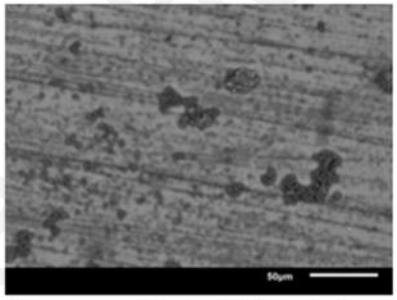

Microstructure of Un-grated Air Annealed Sample w/o Coating

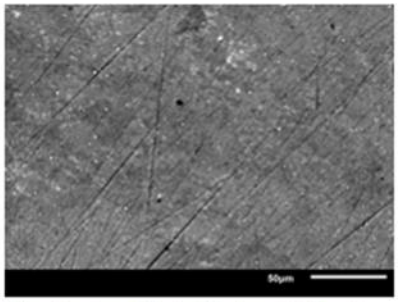

Microstructure of Grated Air Annealed Sample w/o Coating

Figure 37Microstructure of Air Annealed Sample w/o Coating

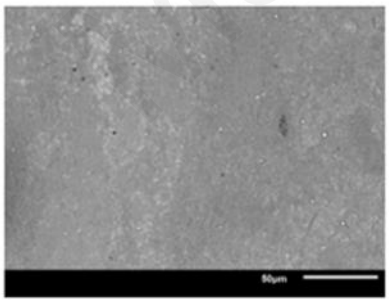

Microstructure of Reference's Sample (Grated)

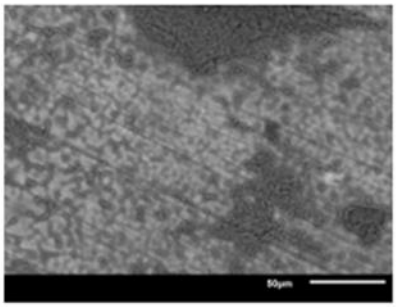

Microstructure of Un-grated Air Annealed Sample with Bison Coating

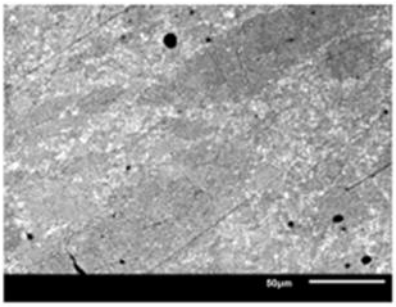

Microstructure of Grated Air Annealed Sample with Bison Coating

Figure 36Microstructure of Air Annealed Sample with Bison Coating

Tables 8 and 9 above, represent the chemical composition of grated and of un-grated air annealed samples, respectively. After heat treatment procedure, air annealed samples are homogeneous with Silicon rich areas (black areas) (Figures 36, 37, 38 and 39).

Generally, as it can be seen from the chemical composition of air annealed samples, there is no change of material's stoichiometry after the heat treatment procedure (Tables 8 and 9).However, comparatively with the other air annealed samples, samples with Soudal and Bison coating have bigger Silicon rich areas (black areas). This can be verified also from the un-grated air annealed samples chemical composition, where compared to nominal composition, there is an important increase at Silicon (Si) values and consequently an important decrease at Tin (Sn) values (Table 9). However, it can be observed from grated sample's microstructures that there are Silicon rich areas (black areas), which can be also verified from grated air annealed sample's chemical composition (Table 8), where compared to nominal composition, there is small increase at Silicon (Si) values and small decrease at Tin (Sn) values.

6.3.3 Thermoelectric (TE) Properties of Air Annealed Samples

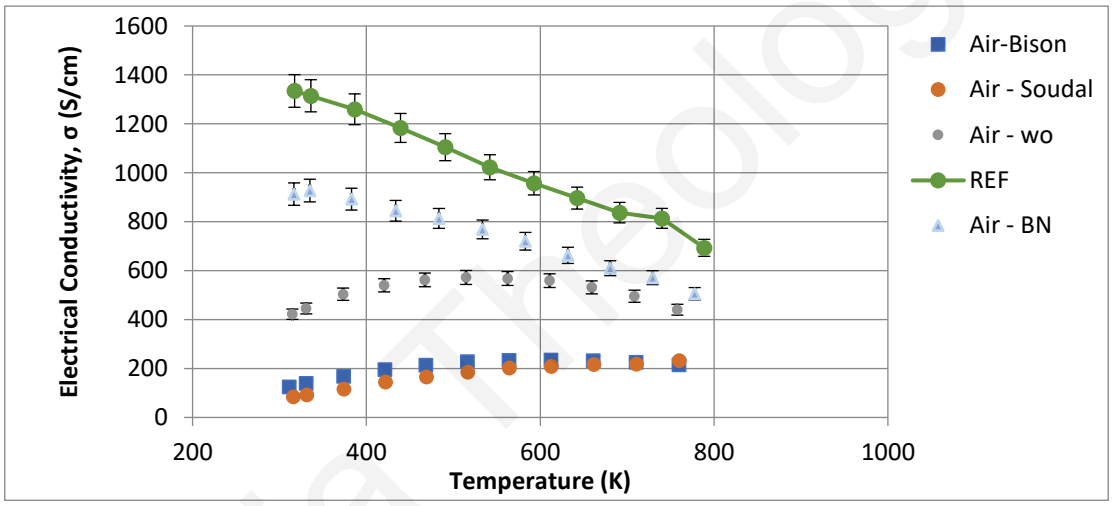

Figure 41Electrical Conductivity against Temperature (Air Annealed Samples)

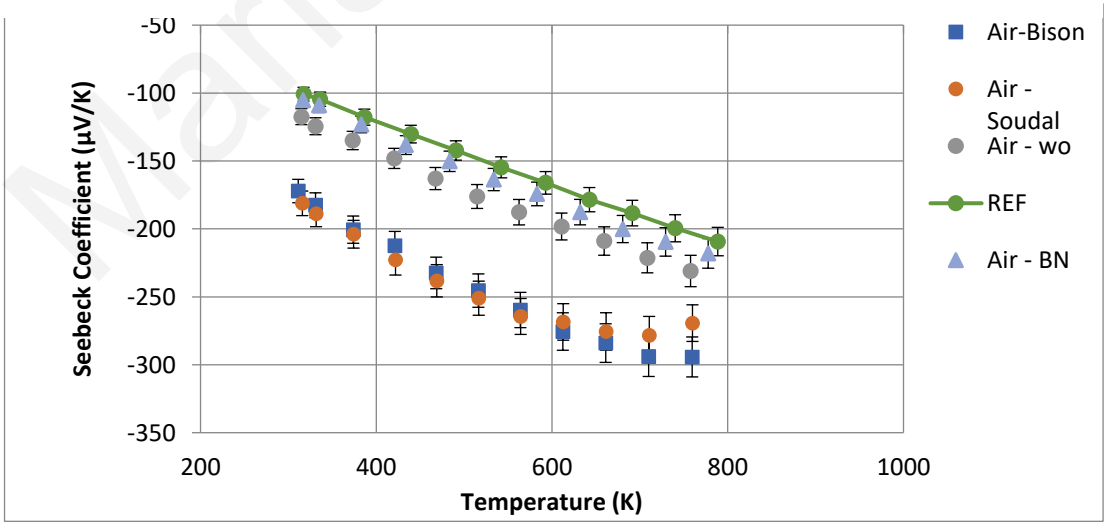

Figure 40Seebeck Coefficient against Temperature (Air Annealed Samples)

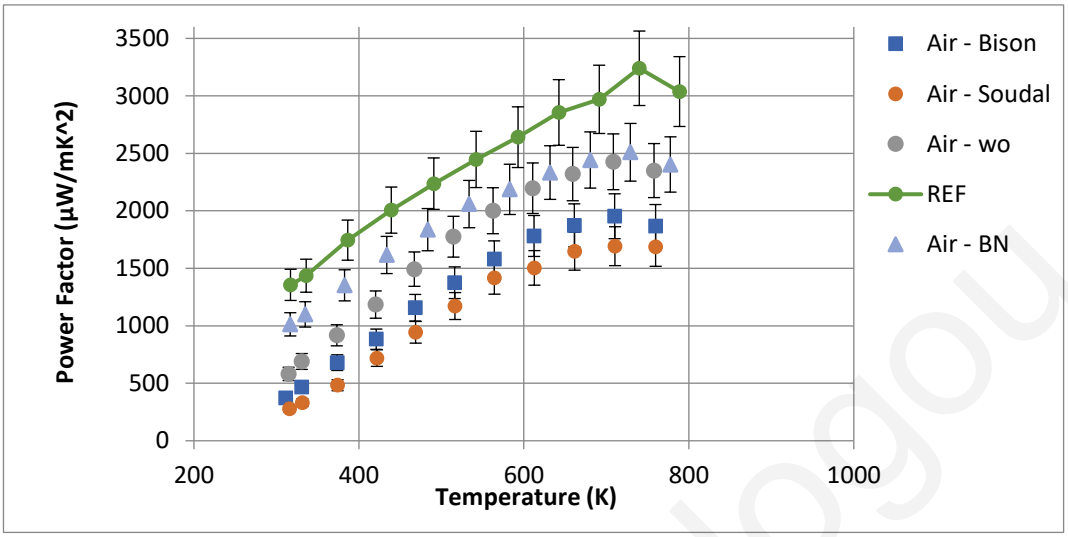

Figure 42Power Factor against Temperature (Air Annealed Samples)

Figures 40, 41 and 42 represent air annealed samples Electrical Conductivity, Seebeck Coefficient and Power Factor parameters. As it can seen from the Electrical Conductivity parameter, all air annealed samples are not in the acceptable range (±5%). (Figure 41) However, at Seebeck Coefficient parameter only one of the air annealed samples is in the acceptable range of ±5%, the sample with BN coating. (Figure 40) Additionally, at Power Factor parameter, air annealed sample with BN coating is in the acceptable range (±5%) but only for a specific period. The specific annealed sample is in the acceptable range of error only for the period of 500 until 720 K. (Figure 42)

Generally, as can be observed from graph's parameters, air annealed samples with Bison and Soudal coatings are the most affected from the heat treatment procedure. However, air annealed sample with BN coating is the least affected from heat treatment in contrast with other air annealed samples.

7 Conclusions

Thermal stability of n-type $Mg_2Si_{0.57}Sn_{0.4}Bi_{0.03}$ was studied as a function of heat treatment in different conditions. For argon and air annealed samples X-ray diffractions patterns, nothing unusual has been observed. As argon annealed samples, air annealed samples have well-formed $Mg_2Si_{0.4}Sn_{0.6}$ solid solutions with high homogeneity. Throughout the entire sample's heat treatment, a small amount of MgO impurity was observed (XRD patterns). As it was mentioned before, for all the Mg_2Si-based materials, MgO impurity is common. However, argon annealed sample with Soudal coating (un-grated) has formed different solid solutions, compared with other annealed samples. Furthermore, a bigger amount of MgO impurity and solid solutions of Si and Sn were formed. Additionally, a big amount of an unknown material was formed. The unknown formed material in the specific argon annealed sample confirms that Soudal coating was diffused at annealed sample's surface. This fact leads to the conclusion that Soudal coating could not protect the sample from the heat treatment procedure.

Considering the annealed samples microstructure after the heat treatment procedure, annealed samples are homogeneous with Silicon rich areas (black areas). Furthermore, as it can be seen from the chemical composition of the annealed samples, there is no change of material's stoichiometry after the heat treatment procedure. However, comparatively with the other annealed samples, samples with Soudal and Bison coating have bigger Silicon rich areas (black areas). This can be verified also from annealed samples chemical composition, where compared to nominal composition, there is an important increase at Silicon (Si) values and consequently an important decrease at Tin (Sn) values.

By studding TE properties of annealed samples after heat treatment, it can be concluded that all annealed samples have been affected to some extent. Generally, air annealed samples were affected the most in contrast with argon annealed samples which were affected the least. Specifically, air annealed samples with Soudal and Bison coatings are the most affected. This fact confirms the inability of the specific coatings to protect the samples from the heat treatment procedure.

Taking into consideration the Seebeck Coefficient and Power Factor parameters, annealed samples with BN (argon), BN (air) and w/o (argon) are the least affected, in contrast with the other annealed samples, which are in the acceptable range (±5% and ±10% respectively). However, in terms of Electrical Conductivity parameter, only argon annealed sample with BN coating is in the acceptable range (±5%). In comparison with other annealed samples, argon annealed sample with BN coating has been the least affected in contrast, with air annealed samples with Soudal and Bison coating which are the most affected from the heat treatment procedure. This fact confirms the inability of the specific coatings to protect the annealed sample from oxidation and Mg loss. As it can be observed from annealed samples TE parameters, when temperature value increases, error between annealed samples and non annealed sample increases too. Additionally, while temperature rises, a drop of sample's Electrical Conductivity and Seebeck Coefficient values can be observed.

In conclusion, argon annealed samples were less affected from the heat treatment, compared to air annealed samples. Furthermore, argon annealed sample's microstructure with Boron Nitride (BN) coating and without coating, are homogeneous and with less Silicon rich areas (black areas) compared with the other annealed samples.

Bison and Soudal coatings could not protect the synthesized material from oxidation and Mg loss after heat treatment. In contrasts, argon annealed samples with BN coating and without coating were less

affected from the specific procedure. Specifically, argon annealed sample with BN coating have been the least affected from the annealed samples. Additionally, can be conclude that by applying coatings such as Boron Nitride (BN) is an effective way to minimize oxidation and Mg loss from heat treatment.

8 References

1. Zhang, X. and Zhao, L., 2015. Thermoelectric materials: Energy conversion between heat and electricity. Journal of Materiomics, 1(2), pp.92-105.
2. L. Zhao, V. P. Dravid and M. G. Kanatzidis. Energy Environ. Sci, 2014 Vol. 7, 251-268.
3. Rafferty, J., Zeidan, A. and Ray, M., 1998. Thomas Johann Seebeck | German Physicist Encyclopedia Britannica
4. Poudel, B., Hao, Q.,Ma, Y., Lan, Y., Minnich, A., Yu, B., Yan, X., Wang, D., Muto, A., Vashaee, D., Chen, X., Liu, J., Dresselhaus, M.S., Chen, G., Ren, Z. Science 2008.
5. Mahan, J., 2015. What Is Resistivity - Formula & Units, Electronics Notes.
6. M.R. Ward (1971) Electrical Engineering Science, pp. 36–40, McGraw-Hill.
7. Matula, R.A. (1979). "Electrical resistivity of copper, gold, palladium, and silver". Journal of Physical and Chemical.
8. J.R. Tyldesley (1975) An introduction to Tensor Analysis: For Engineers and Applied Scientists, Longman, ISBN 0-582-44355-5
9. NETZSCH Analyzing & Testing. 2020. Specific Heat Capacity (Cp).
10. Lewis, M., 1996. Heat transfer mechanisms. Physical Properties of Foods and Food Processing Systems, pp.246-291.
11. Demirel, Y., 2014. Transport and Rate Processes. Nonequilibrium Thermodynamics, pp.75-118.
12. Bird, Stewart, & Lightfoot, pp. 270-271
    Lindon C. Thomas (1992), Heat Transfer, Prentice Hall, p. 8, ISBN 978-0133849424
13. Vengatesan, M., Varghese, A. and Mittal, V., 2018. Thermal Properties Of Thermoset Polymers , Abu Dhabi, United Arab Emirates
14. Ulvac.com. 2020. ULVAC.
15. Whan, R. and Arnold, M., 1986. Materials Characterization. Materials Characterization.
16. Ginzburg, B., 2005. X-ray Diffraction Analysis of C [sub-60] Fullerene Powder and Fullerene Soot. Technical Physics, 50(11), p.1458.
17. Stokes, Debbie J. (2008). Principles and Practice of Variable Pressure Environmental Scanning Electron Microscopy (VP-ESEM). Chichester: John Wiley & Sons. ISBN 978-0470758748.
18. McMullan, D. (1953). "An improved scanning electron microscope for opaque specimens". Proceedings of the IEE - Part II: Power Engineering. 100 (75): 245–256. doi:10.1049/pi-2.1953.0095.
19. Thermoelectrics Handbook: Macro to Nano by D.M. Rowe (2005).
20. CRC Handbook of Thermoelectrics, Ed. M. Rowe, 1995
21. Thermoelectric. 2020. Ferrotec Multi-Stage Deep Cooling Peltier Thermoelectric Cooler Modules.
22. R.A. Taylor and G. Solbrekken, “Comprensive system-level optimization of thermoelectric devices for electronic cooling applications” IEEE Transactions on Components and Packaging Technologies,pp. 23-31, March 2008.
23. C.WOOD Materials for thermoelectric energy conversion, Rep. Prog. Phys., 51(4), 459 (1988).
24. Farahi, N., Stiewe, C., Truong, D., de Boor, J. and Müller, E., 2019. High efficiency Mg2 (Si,Sn)-based thermoelectric materials: scale-up synthesis, functional homogeneity, and thermal stability. *RSC Advances*, 9(40), pp.23021-23028.

25. Hirayama, Naomi (2019). "Substitutional and interstitial impurity p-type doping of thermoelectric Mg2Si: a theoretical study". Sci. Technol. Adv. Mater. 20 (1): 160–172.
26. J. I. Tani and H. Kido, Phys. B, 2005, 364, 218–224.
27. J.E. Mahan, A. Vantomme, G. Langouche, Phys. Rev. B 54 (1996) 965.
28. G. Frommeyer, S. Beer, K.V. Oldenburg, Z. Metallkd. 85 (1994) 372.
29. M. Baleva, G. Zlateva, A. Aranassov, M. Abrashev, E. Goranova, Phys. Rev. B 72 (2005).
30. Yu, B., Chen, D., Tang, Q., Wang, C., & Shi, D. (2010). Structural, electronic, elastic and thermal properties of Mg2Si. Journal of Physics and Chemistry of Solids, 71(5), 758–763.
31. B. Poudel, Q. Hao, Y. Ma, Y. Lan, A. Minnich, B. Yu, X. Yan, D. Wang, A. Muto, D. Vashaee, X. Chen, J. Liu, M. S. Dresselhaus, G. Chen and Z. Ren, Science, 2008, 320.
32. Hirayama, Naomi; Iida, Tsutomu; Sakamoto, Mariko; Nishio, Keishi; Hamada, Noriaki (2019). "Substitutional and interstitial impurity p-type doping of thermoelectric Mg2Si: A theoretical study". Science and Technology of Advanced Materials. 20 (1): 160–172. doi:10.1080/14686996.2019.1580537
33. Khan, A.U.; Vlachos, N; Kyratsi, Th (2013). "High thermoelectric figure of merit of Mg2Si0.55-xSn0.4Ge0.05 materials doped with Bi and Sb". Scripta Materialia. 69 (8): 606–609. doi:10.1016/j.scriptamat.2013.07.008.
34. Polymeris, G., Vlachos, N., Symeou, E. and Kyratsi, T., 2018. Thermoelectric Properties of Bi-Doped Mg2Si0.6Sn0.4Solid Solutions Synthesized by Two-Step Low Temperature Reaction Combined with Hot Pressing.
35. Byjus.com. 2021. GDPR.
36. Yi, T., Chen, S., Li, S., Yang, H., Bux, S., Bian, Z., Katcho, N., Shakouri, A., Mingo, N., Fleurial, J., Browning, N. and Kauzlarich, S., 2012. Synthesis and characterization of Mg2Si/Si nanocomposites prepared from MgH2 and silicon, and their thermoelectric properties. Journal of Materials Chemistry.
37. Haynes, William M., ed. (2011). CRC Handbook of Chemistry and Physics (92nd ed.), Boca Raton, FL: CRC Press. ISBN 1439855110.
38. Fritsch-international.com. 2021. Planetary Mono Mill PULVERISETTE 6 classic line / Description.
39. X. F. Zheng, C.X. Liu, Y.Y. Yan, and Q. Wang, "A review of thermoelectric research –Recent developments and potentials for sustainable and renewable energy applications" Renewable and Sustainable Energy Reviews, Vol. 32(C).
40. Patidar, S., 2018. Applications of Thermoelectric Energy: A Review. International Journal for Research in Applied Science and Engineering Technology, 6(5).
41. Abbasi, V. and Tabar, V., 2020. Measurement and evaluation of produced energy by thermoelectric generator in vehicle. Measurement, 149.
42. Król-Morkisz, K., Karaś, E., Majka, T., Pielichowski, K. and Pielichowska, K., 2019. Thermal Stabilization of Polyoxymethylene by PEG-Functionalized Hydroxyapatite: Examining the Effects of Reduced Formaldehyde Release and Enhanced Bioactivity. Advances in Polymer Technology, 2019.
43. Khan A U et al 2013 Scr. Mater, Volume 69, p. 606
44. Zaitsev V K et al 2006 Phys. Rev. B, Volume 74, p. 045-207
45. Sadia, Y. and Gelbstein, Y., 2012. Silicon-Rich Higher Manganese Silicides for Thermoelectric Applications. Journal of Electronic Materials, 41(6).

46. Fiameni, S., Famengo, A., Agresti, F., Boldrini, S., Battiston, S., Saleemi, M., Johnsson, M., Toprak, M. and Fabrizio, M., 2014. Effect of Synthesis and Sintering Conditions on the Thermoelectric Properties of n-Doped Mg2Si. *Journal of Electronic Materials*, 43(6).
47. Bux, S., Yeung, M., Toberer, E., Snyder, G., Kaner, R. and Fleurial, J., 2011. Mechanochemical synthesis and thermoelectric properties of high quality magnesium silicide. *Journal of Materials Chemistry*, 21(33).
48. Du, Z., Cui, J., Zhu, T. and Zhao, X., 2013. Thermoelectric properties of Sb-doped Mg2Si0.59Sn0.41solid solutions. *physica status solidi (a)*, 210(11).
49. Ioannou, M., Polymeris, G., Hatzikraniotis, E., Paraskevopoulos, K. and Kyratsi, T., 2014. Effect of Bi-doping and Mg-excess on the thermoelectric properties of Mg2Si materials. *Journal of Physics and Chemistry of Solids*, 75(8).
50. Satyala N et al 2014 Acta Mater., Volume 74, p. 141
51. Tani, J. and Kido, H., 2007. Thermoelectric properties of Sb-doped Mg2Si semiconductors. Intermetallics, 15(9).
52. Battiston S et al 2013 J. Electr. Mater. Volume 42, p. 1956
53. Mars, K., Ihou-Mouko, H., Pont, G., Tobola, J. and Scherrer, H., 2009. Thermoelectric Properties and Electronic Structure of Bi- and Ag-Doped Mg2Si1−x Ge x Compounds. Journal of Electronic Materials, 38(7).
54. Schierning, G., 2015. Concepts for medium-high to high temperature thermoelectric heat-to-electricity conversion: a review of selected materials and basic considerations of module design.
55. You, S.-W., Kim, I.-H., Choi, S.-M., Seo, W.-S., & Kim, S.-U. (2012). Solid-state synthesis and thermoelectric properties of N-type Mg2Si. doi:10.1063/1.4731530
56. Yin K., Zhang Q., Zheng Y., Xianli S., Tang X., and Uher C., 2015. Thermal Stability of $Mg_2Si_{0.3}Sn_{0.7}$ under different heat treatment conditions.
57. Farahi N., Stiewe C., Truong N., Johannes de Boor and Eckhard Muller, 2019. High efficiency Mg2 (Si,Sn)-based thermoelectric materials: scale-up synthesis, functional homogeneity, and thermal stability.